Published in final edited form as:
Nat Metab. 2022 April 01; 4(4): 476–494. doi:10.1038/s42255-022-00561-5.

Dysregulation of macrophage PEPD in obesity determines adipose tissue fibro-inflammation and insulin resistance

V Pellegrinelli[1,*], **S Rodriguez-Cuenca**[1,2], **C Rouault**[3], **E Figueroa-Juarez**[1], **H Schilbert**[4], **S Virtue**[1], **JM Moreno-Navarrete**[5,6,7], **G Bidault**[1], **MC Vázquez-Borrego**[1,8], **AR Dias**[1], **B. Pucker**[4,9], **M Dale**[1], **M Campbell**[1,2], **S Carobbio**[1,10], **YH Lin**[1,11], **M. Vacca**[1,12], **J Aron-Wisnewsky**[3,13], **S Mora**[14,15], **MM Masiero**[16], **A Emmanouilidou**[16], **S Mukhopadhyay**[17], **G Dougan**[18,19], **M den Hoed**[16], **R JF Loos**[20,21,22], **JM Fernández-Real**[5,6,7], **D Chiarugi**[1], **K Clément**[3,13], **A Vidal-Puig**[1,2,10,*]

[1]Wellcome-MRC Institute of Metabolic Science and MRC Metabolic Diseases Unit, University of Cambridge, Cambridge, UK

[2]Cambridge University Nanjing Centre of Technology and Innovation, Nanjing, P.R. of China

[3]Sorbonne University, INSERM, NutriOmique research Unit, Paris, France

[4]Genetics and Genomics of Plants, Centre for Biotechnology (CeBiTec) & Faculty of Biology, Bielefeld University, Bielefeld, Germany

[5]Department of Diabetes, Endocrinology and Nutrition, Girona Biomedical Research Institute (IDIBGI), University Hospital of Girona Dr Josep Trueta, Girona, Spain

[6]Department of Medicine, University of Girona, Girona, Spain

[7]CIBERobn Pathophysiology of Obesity and Nutrition, Institut of Salud Carlos III, Madrid, Spain

[8]Maimonides Institute for Biomedical Research of Cordoba (IMIBIC), Cordoba, Spain

[9]Evolution and Diversity, Department of Plant Sciences, University of Cambridge, Cambridge, UK

[10]Centro de Investigacion Principe Felipe, Valencia, Spain

[11]Department of Surgery, Kaohsiung Chang Gung Memorial Hospital and Chang Gung University College of Medicine, Kaohsiung, Taiwan

[*]Corresponding authors: vp332@medschl.cam.ac.uk; ajv22@medschl.cam.ac.uk Phone: +44 (0)1223 336786 Fax: +44 1223 330598.

Author Contributions.

VP developed the hypothesis, designed the experiments, performed the experimental work, collected, and analysed the data, coordinated, and directed the project, created the images, wrote the manuscript. SRC designed and conducted part of the experimental work and edited the manuscript. CR and J-MM-N performed and analysed human experiments. SV performed the bone marrow transplant in mice and the GC-MS for the detection of imidopeptides. HS, GB, MCV-B, ARD, MD, MC, SC, S Mora, MMM, AE, S Mukhopadhyay, MdH conducted experiments. JA-W and KC supervised enrolment and clinical phenotyping of obese subjects. HS, BP, DC performed bioinformatics analysis. DC also edited the manuscript. GD, RL, JMF and KC provided access to human data and discussed the manuscript. AVP developed the hypothesis, coordinated, and directed the project, wrote the manuscript, is the guarantor of this work and, as such, had full access to all the data in the study and takes responsibility for the integrity of the data and the accuracy of the data analysis. All authors critically reviewed and edited the manuscript. The authors declare no competing interests.

Declaration of interests

The authors declare no competing interests.

Europe PMC Funders Author Manuscripts

[12]Insterdisciplinary Department of Medicine, Università degli Studi di Bari “Aldo Moro”, Bari, Italy

[13]Assistance-Publique Hôpitaux de Paris, Nutrition department, Pitié-Salpêtrière hospital, Paris, France

[14]Dept Biochemistry and Molecular Biomedicine, Faculty of Biology, University of Barcelona, Barcelona, Spain

[15]Institute of Biomedicine, University of Barcelona (IBUB), Barcelona, Spain

[16]The Beijer Laboratory and Department of Immunology, Genetics and Pathology; Uppsala University and SciLifeLab, Uppsala, Sweden

[17]MRC Centre for Transplantation Peter Gorer Department of Immunobiology School of Immunology & Microbial Sciences King's College, London, UK

[18]Cambridge Institute of Therapeutic Immunology and Infectious Disease, Jeffrey Cheah Biomedical Centre, University of Cambridge, Cambridge, UK

[19]Division of Infectious Diseases, Department of Medicine, University of Cambridge, Cambridge, UK

[20]Charles Bronfman Institute for Personalized Medicine, Icahn School of Medicine at Mount Sinai, New York, NY, US

[21]The Mindich Child Health and Development Institute, Icahn School of Medicine at Mount Sinai, New York, NY, US

[22]Novo Nordisk Foundation Center for Basic Metabolic Research, Faculty of Health and Medical Science, University of Copenhagen, Copenhagen, Denmark

Europe PMC Funders Author Manuscripts

Abstract

Resulting from impaired collagen turnover, fibrosis is a hallmark of adipose tissue dysfunction and obesity-associated insulin resistance. Prolidase also known as Peptidase D (PEPD) plays a vital role in collagen turnover by degrading proline-containing dipeptides but its specific functional relevance in adipose tissue is unknown. Here we show that in human and murine obesity, PEPD expression and activity decrease in adipose tissue, and PEPD is released into the systemic circulation, which promotes fibrosis and adipose tissue insulin resistance. Loss of the enzymatic function of PEPD by genetic ablation or pharmacological inhibition causes adipose tissue fibrosis in mice. In addition to its intracellular enzymatic role, secreted extracellular PEPD protein enhances macrophage and adipocyte fibro-inflammatory responses via EGFR signaling, thereby promoting adipose tissue fibrosis and insulin resistance. We further show that decreased prolidase activity is coupled with increased systemic levels of PEPD that act as a pathogenic trigger of adipose tissue fibrosis and insulin resistance. Thus, PEPD produced by macrophages might serve as a biomarker of adipose tissue fibro-inflammation and could represent a therapeutic target for AT fibrosis and obesity-associated insulin resistance and type 2 diabetes.

Keywords

Fibrosis; inflammation; macrophages; Prolidase; PEPD; Xaa-Pro dipeptidase; Obesity; adipose tissue; extracellular matrix; EGFR; exploratory factor analysis

As obesity progresses, sterile inflammation and constitutive activation of pro-fibrotic cells (e.g. macrophages (Mϕ), adipose tissue progenitors) occurs in the adipose tissue (AT) depots, leading to AT fibrosis[1,2]. Fibrosis of the AT impairs adipocyte hypertrophy and hyperplasia adaptations and associates with insulin resistance (IR), and increased risk of type 2 diabetes (T2D)[3,4]. Following bariatric surgery, fibrosis in AT impedes weight loss due to the rigid fibrotic wall constraining the adipocytes and preventing efficient and timely AT lipid mobilisation[5,6]. The degree of AT fibrosis and inflammation (fibro-inflammation) might be a more significant risk factor for metabolic complications than the degree of obesity. Supporting this view, the spectrum of obesity includes severely obese patients that appear to be inappropriately metabolically healthy, in contrast with other mildly overweight patients that exhibit surprisingly severe metabolic complications[7]. GWAS have identified DNA variants dissociating obesity from its metabolic complications helpful to investigate these clinical paradoxes. We and others identified the rs731839 variant in the locus corresponding to Prolidase or Peptidase D (PEPD), influencing lipid and glycaemic profiles[8,9]. The G allele was associated with metabolically unhealthy lipid (higher triglyceride and lower HDL-cholesterol levels) and glycaemic profiles (higher fasting insulin and lower adiponectin levels). Impaired lipid and carbohydrate metabolism were paradoxically associated with lower adiposity[10,11].

PEPD is a homodimer cytosolic protein responsible for degrading proline-containing dipeptides (Xaa-Pro or Xaa-hyp), playing a pivotal role in the final step of collagen degradation and turnover. Complete *PEPD* deficiency in humans is a rare genetic disorder characterised by a complex phenotype of angiopathies and defective wound healing - consistent with impairment of collagen turnover[12]. Impaired collagen turnover in *PEPD* deficient patients leads to pulmonary fibrosis[13].

Evidence from cancer and liver fibro-inflammation stages indicates that PEPD protein is actively secreted, acting as a non-canonical ligand of the EGFR and ErBB2 receptors [14–17]. Therefore, we hypothesised that functional defects in PEPD may be pathogenically relevant in AT through impairing collagen degradation and defects in intracellular signalling mediated by its extracellular and non-enzymatic roles.

We observed decreased PEPD peptidase activity and increased PEPD protein secretion in inflammatory Mϕ and AT from obese individuals and murine models fed on a high-fat diet (HFD). Lower PEPD activity in AT and higher PEPD protein levels in serum are directly proportional to AT fibrosis, inflammation, and metabolic dysfunction. Using pharmacological and genetic murine models to target PEPD peptidase activity and/or its secretion, we show that dysfunctional PEPD intracellular dipeptidase activity induces AT fibrosis, whereas the PEPD secreted by AT is the main contributor to inflammation, IR and metabolic dysfunction. PEPD originated in inflammatory Mϕ, plays an essential role in promoting fibro-inflammatory responses via activation of EGFR in Mϕ and preadipocytes. Moreover, genetic ablation of *pepd* in hematopoietic cells prevented obesity-induced PEPD release and averted AT fibro-inflammation and obesity-associated metabolic dysfunction. Altogether, these data reveal that obesity-associated severity of AT fibro-inflammation

and metabolic disturbances for a given fat mass depend on PEPD activity and PEPD extracellular levels.

Results

Low PA in obese AT associates with high PEPD release, IR and fibrosis

We measured *PEPD* mRNA expression, prolidase activity (PA) and secretion from AT of seven human cohorts spanning a broad spectrum of BMIs, ages, and degrees of IR (Extended data Figure 1a). *PEPD* expression was lower in visceral white AT (VsW) of obese than lean individuals and lower in obese type 2 diabetics than in obese normo-glycaemic patients (Figure 1a, b). *PEPD* mRNA expression was lower in VsW than in subcutaneous white AT (ScW) in a paired sample cohort study (Figure 1c), and lower *PEPD* expression in VsW was associated with higher BMI and collagen content in AT from obese individuals (measured as hydroxyproline levels, HPro) (Figure 1d). Moreover, low *PEPD* expression in VsW was associated with lower expression of AT metabolic genes such as *PLIN1, PPARG* and *GLUT4* (Table 1) and reduced VsW *PEPD* expression in obese individuals was associated with reduced PA in VsW (cohort 2e, f; Figure 1e). Lower PA matched the higher release of PEPD from the VsW of these patients (cohort 2e, f; Figure 1f), suggesting a causal relationship between the reduction of the intracellular enzymatic activity and the enzyme's release. Among obese subjects, those with higher VsW PEPD release were more prone to IR and T2D (Extended data Figure 1b). The ROC curve analysis highlighted that both the PEPD released and low PA in VsW (but not ScW) predicted T2D (cohort 2e, f; Figure 1h; Extended data Figure 1c,d). HigherPEPD release from VsW was coupled with higher PEPD serum levels in obese subjects than lean individuals and was associated with elevated cholesterol and aspartate transaminase (ASAT) levels (Cohort 2e, Figure 1h; Extended data Figure 1e). Re-analysis of serum proteomic data from an independent set of insulin resistant and sensitive obese subjects[18] further confirmed the predictive value of PEPD for IR (Figure 1i). Moreover, serum PEPD levels were positively correlated with lipid metabolism (e.g. APOA proteins), inflammation (e.g. S100A12, DPP4) and ECM related proteins (e.g. TNC, COL4A2) (Figure 1j, k). Altogether, these human data provided evidence for the potential relevance of PEPD as a marker of fibro-inflammation and IR in obese individuals.

A similar pattern of low AT PEPD activity coupled with high circulating levels of PEPD was recapitulated in two independent murine models of obesity (i.e. mice fed HFD45% and HFD58%) (Extended data Figure 1f-m). We found that HFD only affected PEPD peptidase activity in AT but not in the liver or muscle (Extended data Figure 1f, g). In mice fed HFD for 28 weeks, the tissue PA in AT was reduced in the first eight weeks, followed by the release of PEPD (Extended data Figure 1i-k). Despite the increased PEPD serum level, the enzymatic activity of PEPD in serum remained stable during the HFD time course, suggesting that the activity of the enzyme in serum is reduced and might not affect the development of AT fibrosis (Extended data Figure 1l). While the liver contributed to the overall levels of serum PEPD in mice, only the gonadal WAT (GnW) depot showed a significantly increased PEPD release in response to HFD (Figure 1l). Dysregulation in PEPD activity and release were associated with AT fibrosis and metabolic disturbances (e.g.

hyperglycaemia, liver steatosis) (Figure 1m; Extended data Figure 1m). Accordingly, serum levels of PEPD predicted the degree of fibrosis (peri-Ad collagen) and inflammation (*tnfa* expression) in GnW (Figure 1n).

PA inhibition induces PEPD secretion, AT fibrosis and metabolic complications in lean mice

To uncouple the effects of PEPD from obesity, we treated chow-fed lean mice with CBZ-Proline (CBZ-Pro), a pharmacological inhibitor of PEPD activity[19]. CBZ-Pro-treated mice showed higher levels of the dipeptide Glycine-Proline in serum, confirming PEPD activity inhibition, and exhibited higher PEPD serum levels than control mice (Figure 2a, b). CBZ-Pro-treated mice had similar body weight, fat mass and tissue weight than control mice (Extended Data Figure 2b-d). However, despite similar fat mass, they had more severe AT fibro-inflammation in GnW and were more hyperglycaemic, glucose intolerant, and insulin-resistant than controls (Figure 2c-h). Of note, CBZ-Pro-treated mice showed comparable fasting insulin and FFA blood levels (Extended data Figure 2e, f) and no impairment to the expected insulin level increase in response to glucose compared to controls (Extended data Figure 2g). However, the phosphorylated-AKT/total-AKT ratio in non-stimulated conditions was lower in CBZ-Pro-treated mice than controls in both GnW (associated with a slight increase in AKT total) and skeletal muscle, suggesting higher AT and muscle IR (Extended data Figure 2h, i). The amount of PEPD into the serum of CBZ-Pro treated mice was positively correlated with the degree of ScW fibrosis and glycaemia in the fed state (Figure 2i). Altogether, these results show that downregulation of the intracellular PEPD activity in AT and concomitant increase in the serum levels of PEPD induced AT fibro-inflammation and IR. Furthermore, in line with the human GWAS data, dysregulation of PEPD uncoupled fibro-inflammation and metabolic dysfunctions from obesity [8,9,11].

Given this dual role of PEPD, it remained unclear which event – i.e. decreased PEPD intracellular dipeptidase activity or increased PEPD released from the cells- was primarily responsible for AT fibrosis and/or metabolic alterations. We performed an Exploratory Factor Analysis (EFA) to investigate how serum PEPD level/PEPD activity co-varied with the metabolic parameters measured in the CBZ-Pro-treated mice and controls (Figure 2j). EFA showed that factor 1, representing a cluster of AT fibrosis-related variables, co-varied with PEPD serum levels and fed glucose levels. Moreover, factor 2, the cluster of "obesity"-related variables (adiposity, glycaemia, and steatosis), also co-varied with PEPD serum levels, whereas factor 3 showed that the activity of GnW PEPD co-varied with fasting glucose. Therefore, EFA indicated that the serum level of PEPD might explain the "fibrotic" profile and hyperglycaemic status observed in CBZ-Pro mice.

The link between serum PEPD, fibrosis and glycaemia was further strengthened when we included the CBZ-Pro mice fed HFD 58% data in the EFA (Factor 1, Extended data Figure 2i). However, the co-variation between PEPD serum level and "obesity"-related variables was not sustained (Extended data Figure 2j). We rationalised that since HFD *per se* down-regulates PEPD activity/increases its secretion, it was likely that HFD-fed control mice might have developed fibro-inflammation as in CBZ-Pro-treated mice, matching the pro-fibrotic effects of this PEPD pharmacological inhibitor observed in chow-fed conditions.

Confirming this interpretation, untreated control and CBZ-Pro-treated mice fed HFD 58% exhibited similar severe AT collagen deposition, fasting insulin, FFA and glucose levels, and insulin intolerance (Extended data Figure 2e, f, k-m).

Global *Pepd* ablation worsens obesity-associated AT fibrosis and metabolic comorbidities

To dissect the role of inhibition of PEPD activity from the extracellular action of the released PEPD, we phenotyped the global *pepd* heterozygote (HET, +/-) and knock-out (KO, -/-) mice against wild type (WT, +/+) littermates. PEPD activity and serum levels were not detected in the total KO. Interestingly, *Pepd* HET mice showed 50% decreased PEPD activity, but no differences in PEPD serum levels compared to WTs (Figure 3a,b; Extended data Figure 3a,b), and were anatomically similar (i.e. length, BW, fat mass and tissue weight; extended data Figure 3c-f). In contrast, *pepd* KO exhibited a runty phenotype characterised by short length, low body weight, and decreased fat mass (Extended data Figure 3c-f), making subsequent phenotyping difficult and of limited value to assess metabolism. Therefore, *pepd* HET mice were subsequently metabolically phenotyped.

Higher collagen accumulation was observed in ScW (HET/KO) and GnW (KO) compared to WT littermates fed a chow diet, supporting the role of reduced PEPD activity in promoting fibrosis (Figure 3c), an association strengthened by correlation matrix analysis (Extended Data Figure 3g). Moreover, EFA analysis of chow-fed *pepd* mice showed that Factor 1, clustering GnW or ScW fibrosis-related variables, had strong loading of glucose blood levels and negative loading of PEPD activity in AT depots (Figure 3d). Additionally, correlation matrix analysis showed a positive association between AT fibrosis and IR (Extended data Figure 3g). *Pepd* HET showed similar glucose, FFA levels, and glucose and insulin tolerance than WT mice despite lower fasting insulin levels (Extended data Figure 3h-k). However, we found that insulin-induced AKT phosphorylation was lower in both GnW and liver from *pepd* HET chow-fed mice than WTs, with no observed differences in skeletal muscle (Extended data Figure 3l-n).

The development of metabolic complications in *pepd* HET mice (i.e. IR, increased fasting FFA and liver steatosis) exacerbated on HFD compared to chow diet. There were no differences in BW among genotypes following HFD feeding (Extended data Figure 4a). *Pepd* HET mice fed HFD 45% resulted in higher fed glucose levels and insulin intolerance than WT mice, despite maintaining similar fasted glucose, insulin and FFA levels (Extended data Figure 4b-d). When challenged with HFD 58%[20] *pepd* HET mice exhibited greater fibro-inflammation in GnW than HFD 45% (Extended data Figure 4e, f) and demonstrated a trend to glucose and insulin intolerance despite showing lower fasting glucose than WT mice (Figure 3e-g). *Pepd* HET mice also showed higher FFA levels than controls (Figure 3g). In addition, the basal AKT phosphorylation in GnW was decreased in *pepd* HET, and the AT-IR index[21] was higher than in WT mice (Figure3h, i). Similarly, the liver *of pepd* HET mice exhibited more steatosis than WT (Figure 3j). Of note, the basal AKT phosphorylation in gastrocnemius muscle was not significantly different in *Pepd* HET mice fed either chow or HFD(Extended data Figure 4g). Collectively, these results indicate that reduced PEPD activity in *pepd* HET mice was sufficient to develop AT fibrosis in the absence of obesity and that HFD further exacerbated metabolic complications. Moreover, EFA revealed that IR

and liver steatosis could be linked to BW and GnW fibrosis in *pepd* HET mice fed either chow or HFD (45% and 58%), as these variables clustered and co-varied together (Factor 2, Figure 3k).

To unmask the molecular mechanisms underlying the fibrogenic and pathogenic effectors driven by the downregulation of *pepd*, we performed RNA-Sequencing for GnW and liver of *pepd* HET and KO mice, fed chow and HFD 45%. Of relevance, gene expression profiling of the gastrocnemius muscle did not differ in *pepd* mice among genotypes and dietary interventions (Extended data Figure 4h). The 45%HFD nutritional challenge was selected to prevent the confounding fibro-inflammatory effect resulting from 58% HFD down-regulating *pepd* in WT mice (Extended data Figure 4i). Analysis of DEGs and the top differentially regulated pathways in GnW *pepd* HET and KO mice (fed 45 %HFD) *vs* WT revealed that *pepd* HET and KO mice had higher expression of genes involved in actin cytoskeleton and cell cycle regulation, immune system, inflammatory-related pathways, and ECM/ECM organisation-related proteins (Figure 4a, Extended data Figure 4j; Table S2a-S5a). Also, *pepd* HET mice fed HFD 45% showed lower expression of genes involved in metabolic pathways, including fatty acids, leptin, and insulin signalling. The *pepd* KO mice showed higher expression of genes in the pro-diabetes-related cluster. Validation of these data using additional *in vitro* and *ex-vivo* experiments confirmed that partial or total *pepd* ablation results in AT dysfunction characterised by impaired adipogenesis from GnW progenitors, lipolysis in mature adipocytes, and leptin secretion from GnW tissue explants (Figure 4b-f).

Next, we focused on analysing the DEGs related to AT function and fibro-inflammation regulated by HFD 45% on each genotype (Figure 4g; Table S6a-S8a). In response to HFD 45% and compared with chow diet, GnW of the *pepd* HET mice exhibited higher expression of pro-fibrotic, ECM components, ECM remodelling genes, inflammatory and immune cells and lower expression of metabolic genes.

Extending the transcriptomic analysis to the liver, we observed an enrichment of the DEGs related to “Immune system” related pathways – mainly T cell-related pathways -were up-regulated in *pepd* KO and HET compared to WT in HFD45% fed mice. “Diabetes” pathway was also enriched in the DEGs up-regulated in *pepd* KO versus WT. However, “Matrisome” and “collagen formation” pathways were downregulated in both *pepd* KO and HET livers compared to WT (Figure4h, extended data Figure 4k; Table S2b-S5b). Further analysis of the DEGs related to fibro-inflammationand steatosis did not reveal significant differences between *pepd* HET and WT mice in response to HFD (Figure 4i; Table S6b-S8b). These results align with the absence of liver fibrosis in *pepd* ablated mice fed HFD45% (Figure 4j). However, *pepd* HET mice showed a more significant up-regulation of pro-steatosis markers in response to HFD (i.e. β-oxidation and cholesterol metabolism) than WT (Figure 4i; Table S6b-S8b).

Collectively, transcriptomic analyses in GnW and liver confirmed exacerbated GnW fibro-inflammation and dysfunction in both the KO and HET mice when challenged with HFD 45%. The GnW fibro-inflammatory response to HFD was stronger in *pepd* HET mice than in WT. Notably, fibro-inflammation was not exacerbated in the liver of *pepd*-ablated mice.

This supports the relevance of PEPD in ECM remodelling of the AT when challenged with HFD and suggests that hepatosteatosis observed in *pepd* HET mice might not directly result from ablation of *pepd* in the liver but as a consequence of AT dysfunction and fibro-inflammation.

The strong pro-inflammatory fingerprint observed in the RNAseq suggested that GnW Mϕ and immune cell-derived factors might contribute to the metabolic phenotypes associated with the genetic ablation of *pepd* in AT, pointing to a pathogenic link between PEPD dysregulation and immune regulation. Cellular fractionation of GnW from lean mice revealed that Mϕ (CD11b+) reported the highest levels of *pepd* expression compared to mature adipocytes (AD), other immune (CD45+), endothelial cells (CD31+) or stroma-vascular fractions (SVF) (Figure 5a). Moreover, PEPD activity increased during Mϕ differentiation using bone-marrow-derived Mϕ (BMDMs) (Extended data Figure 5a). Consistent with the results from total AT, the expression of *pepd* was lower in AT Mϕ from 16 weeks-old ob/ob mice and mice fed 20 weeks with HFD 45% compared with their controls (genetically lean and chow-fed mice) (Figure 5b; Extended data Figure 5b). These findings were validated in humans by showing enrichment of PEPD in human AT's immune cells (CD45+) (Figure 5c). Reanalysis of proteomic data from human-induced pluripotent stem cell-derived Mϕ (iPSDM, PXD001953[22]), confirmed the high abundance of PEPD in Mϕ compared to undifferentiated iPSCs (Extended data Figure 5c). Given that obesity is associated with an imbalance between classically activated Mϕ (inflammatory) and alternatively activated Mϕ (non-inflammatory), we assessed the modulation of *pepd* expression by specific Mϕ polarising agents[23]. In keeping with the reduction of *pepd* expression in inflamed AT of obese mice, *pepd* expression was also lower in pro-inflammatory M(LPS) cells, whereas it was higher in M(GC) and not modulated in M(IL-4) treated cells compared to unstimulated Mϕ (Extended data Figure 5d). Additional evidence of the relevance of human Mϕ was provided by RNA-Seq comparing undifferentiated human inducedpluripotent stem cells (iPSCs) and differentiated and analysis of the effect of LPS on human macrophage-derived monocytes (MDM) and iPSDM (EGAS00001000563)[24]. In line with murine models, stem cell transcriptomic analysis confirmed that i) *PEPD* expression increases during human Mϕ differentiation; ii) iPSDM and MDM display similar *PEPD* expression levels; and iii) PEPD expression decreases in response to LPS in both iPSDM and MDM (Figure 5d). We then validated at the cellular level that BMDMs treated with CBZ-Proline or LPS decreased PEPD activity (Figure 5e) and increased PEPD released to the medium compared to non-activated or activated Mϕ (Figure 5f; Extended data Figure 5e-g). These results strengthen the functional coupling between the lower enzymatic activity of PEPD in AT and the higher release of PEPD to the extracellular compartment. Interestingly, higher PEPD release from LPS-activated BMDMs was not associated with higher PA in the culture media, suggesting that released PEPD might exhibit reduced PA following posttranslational modifications (Extended data Figure 5h).

Pepd ablation in hematopoietic cells uncouples AT fibrosis from metabolic alterations

To dissect the pivotal role of PEPD secreted from Mϕ driving fibro-inflammation and metabolic disturbances, we performed a bone marrow transplant (BMT) from *pepd* KO into WT recipient mice to ablate *pepd* exclusively in hematopoietic cells (HCs) (Figure

5g, h). BMT is commonly used in the literature to target AT macrophages (ATM)[25–27] as approx. 85% of the ATM originate from the bone marrow[28]. Thus, BMT KO mice showed similar adiposity to BMT WT mice (when fed chow diet). BMT KO mice showed reduced PA of 85% in peritoneal Mϕ and 50% in the whole AT (Figure 5i, j). As anticipated, the reduction in PEPD activity by genetic manipulation was not associated with increased PEPD levels in serum. This contrasted with the increase observed in secreted PEPD levels in CBZ-Pro-treated mice or dietary models of obesity (Figure 5k). As previously seen in models with global decreased PEPD activity, the BMT KO also had increased collagen accumulation in AT compared to BMT WT (Figure 5l). However, the BMT KO mice maintained carbohydrate metabolic homeostasis in contrast to the chow-fed CBZ-Pro-treated mice, in which the decreased PEPD activity was inversely associated with PEPD secretion (Extended data Figure 5i-n). Of note, BMT KO mice adiposity was marginally lower than WTs when fed a chow diet but it was significantly lower when fed 58% HFD (Extended data Figure 5o-q). Furthermore, when fed 58% HFD, the BMT KO mice exhibited more fibrosis than WTs but were resistant to obesity and associated metabolic disturbances (i.e. glucose and insulin tolerance, AT IR and liver steatosis) (Figure 5l-o), Extended data Figure 5r,s). In addition, while GnW showed reduced fibro-inflammatory markers expression, liver and skeletal muscle did not show significant changes at thegene expression level, reinforcing the importance of Mϕ PEPD of the GnW in regulating metabolic functions (Figure 5p). Thus, the BMT KO model exhibited increased AT fibrosis uncoupled from metabolic complications such as IR and liver steatosis, and pointed to the relevance of the extracellular PEPD produced by Mϕ as a critical trigger of fibro-inflammation and metabolic complications. Moreover, EFA run for BMT chow fed mice confirmed the negative association between AT fibrosis and PEPD enzymatic activity (Factor 1, Figure 5q), and factor 3 showed that AT IR-related parameters (i.e. AT-IR and FFA levels) co-varied with PEPD serum levels (Figure 5q). Thus, these results supported that extracellular PEPD might be an essential trigger of AT fibro-inflammation and related metabolic dysfunctions.

We investigated whether the released PEPD “per se” was a determinant of Mϕ polarisation and could trigger inflammation. Treatment of Mϕ with purified PEPD protein-induced phosphorylation of NF-κB (ser536) and the expression of inflammatory markers, such as *cox2* and *il-lβ*, while non-inflammatory markers *mgl1* and *mrc2* were downregulated (Figure 6a; extended data Figure 6d). Phospho-kinase proteome analysis using a profiler array on PEPD-treated BMDMs confirmed that PEPD phosphorylated EGFR (Extended data Figure 6e,f)[15]. Pre-treatment of Mϕ with Erlotinib, an EGFR-specific tyrosine kinase inhibitor, attenuated PEPD induced NFκB phosphorylation, as well as *cox2* and *il1β* expression (Figure 6b, c; extended data Figure 6g). We further confirmed this association by showing that PEPD-induced *Cox2* and *Il1β* expression was reduced in response to *Egfr* silencing (~75%) (Extended data Figure 6h-j).

Purified PEPD promotes AT fibro-inflammation and IR

Using *Tabula Muris* Database[29], we observed that AT, liver, and muscle were the organs with the highest *Egfr* expression(Extended data Figure 6k). We rationalised that secreted PEPD from Mϕ could also signal to other cells in AT or other organs through EGFR-dependent pathways. To test the effect of PEPD at the whole organism level, C57Bl/6N chow-fed

mice were injected intraperitoneally with purified PEPD protein three times a week for six weeks. We investigated the gene expression of *Cox2*, known to be induced by PEPD through EGFR-dependent pathways [15] and found that GnW showed the most significant increase in *Cox2* expression (Figure 6l). Following injection of PEPD, the tissular PA remained unchanged compared to control mice (Extended Data Figure 6m), indicating that the effects observed in mice injected were independent of its enzymatic activity. While BW, body composition, ITT and GTT were unaltered upon PEPD injection (Figure 6d; Extended data Figure 6n-r), we observed active tissue remodelling, notably in the GnW, withincreased peri-adipocyte (peri-AD) fibrosis in PEPD-injected mice compared to control (Figure 6e). Of relevance, the collagen and ECM remodelling enzymes' mRNA expression were strongly downregulated, suggesting the existence of compensatory mechanisms (Figure 6f, g). We observed higher presence of crown-like structures around adipocytes close to high expression of "M2 tissue remodelling" Mϕ markers in PEPD-injected mice compared to controls (Figure e, g). Expression of adipocyte markers was reduced in AT from PEPD injected mice (Figure 6h), and both basal AKT phosphorylation levels and GLUT4 protein expression were reduced in GnW, indicative of reduced AT insulin sensitivity (Figure 6i).

In support of these *in vivo* results, we characterised *in vitro* the effect of added extracellular PEPD on differentiated and non-differentiated preadipocytes, considered critical pro-fibrotic cellular effectors in the AT[30,31], and on mature primary adipocytes. Supporting a direct pro-inflammatory role, purified PEPD increased *il-6* expression in differentiated preadipocytes, promoted the production of collagen I, and prevented lipid accumulation in preadipocytes in part through a mechanism involving EGFR signalling (Extended data Figure 7a). Purified PEPD protein also induced IL-6 release from mature adipocytes (Extended data Figure 7b). However, whilst purified PEPD increased mRNA expression of inflammatory markers and deposition of collagen from hepatic stellate cells *in vitro*, we did not observe any effect on liver fibrosis or lipid accumulation, nor changes in gene expression profile (of functional, inflammatory, and fibrotic genes) in the liver in vivo (Extended data Figure 7c-g). Similarly, we did not observe any effect on skeletal muscle fibro-inflammation, despite higher mRNA expression of *Tnfα* compared to control mice (Extended data Figure 7h, i). *In vitro*, PEPD had a mild effect on muscle fibroblasts, inducing *cox2* and *cyclin D1* expression (Extended data Figure 7j). These effects were reversed in response to Erlotinib, supporting the role of EGFR as a mediator of PEPD effects. While PEPD did not modify collagen production in muscle, we found that it did increase αSMA protein expression suggesting activation of fibroblasts in response to exogenous PEPD. Nevertheless, this effect on αSMA staining was not reversed in Erlotinib's presence (Extended data Figure 7k). Altogether, these results suggest that purified PEPD treatment targeted GnW inducing severe tissue remodelling and IR. Moreover, EFA supported a causal relationship between serum PEPD levels, insulin sensitivity (Factor 1) and GnW fibrosis (Factor 2) (Figure 6j).

Secreted PEPD is the primary pathogenic factor in fibro-inflammation

To dissect the main pathogenic factors linking specific PEPD dysregulation and metabolic and fibro-inflammatory differences, we performed a global integrative Correlation Matrix Analysis and EFA, integrating the four PEPD *in vivo* experimental models (pharmacological, genetic, macrophage-specific genetic ablation and exogenous PEPD

treatment). Correlation analysis, including either chow-fed mice alone or with HFD-fed animals, revealed a negative correlation between the level of AT fibrosis and PEPD activity accounting for the reduced AT PEPD activity and fibrosis in these models (except the PEPD injection experiment) (Extended data Figure 8b,c). In agreement with this, EFA performed in chow-fed mice showed that Factor 3, clustering AT fibrosis-related variables, had negative loading of AT PEPD activity and body weight (Extended data Figure 8a). This inverse relationship was observed between AT fibrosis and PEPD activity when EFA included chow+HFD fed animals (Factor 4, Figure 7a). We then transformed the data to plot and visualise in two dimensions the relationship between the variables (Figure 7b, extended data Figure 8d) and the animal models. We observed that CBZ-Pro and BMT mice diverged in dimension 4 (corresponding to factor4), in which Fibrosis co-varied negatively with both PEPD activity and serum level, i.e. fibrosis could be explained by the absence of PEPD (Figure 7c). This association is consistent with the fact that in contrast to BMT KO mice with no PEPD released from Mϕ, the CBZ-Pro mice displayed a higher release of PEPD. Of relevance, they also differed in terms of insulin sensitivity status. Therefore, these data strengthen the role of PEPD released from Mϕ in promoting IR. Factor 3, clustering ScW vascular fibrosis and glucose levels, had high loading of PEPD serum levels (Figure 7a). Interestingly, *pepd* HET mice fed HFD58% and PEPD-injected mice overlapped in this dimension (Dim 3), suggesting similarities between these two models regarding the role of serum PEPD in promoting AT fibrosis (Figure 7c). Of note, these two models also shared AT IR. However, *pepd* HET fed HFD58% and PEPD-injected mice diverged in dimension 1 (corresponding to factor 1), in which the insulin sensitivity status could be explained by adiposity (Figure 7a, d). Indeed, while both models displayed AT IR, *pepd* HET mice fed HFD were obese while PEPD-injected mice remained lean. Finally, *pepd* KO and both CBZ-Pro/PEPD-injected mice diverged on dimension 2 (corresponding to factor 2) in which GnW fibrosis and FFA levels co-varied with PEPD serum levels, i.e. AT fibrosis and higher FFA levels could be explained by higher PEPD serum level (Figure 7a, d). Therefore *pepd* KO mice differed from CBZ-pro and PEPD-injected mice because displaying higher PEPD serum levels exacerbated metabolic complications and fibrosis deposition in GnW.

Discussion

Departing from human GWAS identifying PEPD as a potential causal gene of IR and dyslipidaemia [8,9,11], we focused on its role in metabolic organs in the context of obesity. In obesity, PEPD was downregulated exclusively in AT, notably in the gonadal depot, where we posited that it would play a central role, but not in skeletal muscle or liver. A critical observation was that the lower the PA in GnW (or the visceral depot in humans), the higher the PEPD levels detected in the serum of obese mice and humans. The liver appeared to be an essential organ contributing to serum levels of PEPD. However, gonadal fat was the only tissue where PEPD released is altered by HFD. We, therefore, hypothesised that the higher PEPD serum level observed in obese subjects might reflect the release of PEPD from the GnW. Our *in vivo* and *in vitro* time course HFD and LPS treatment, respectively, suggest that the release of PEPD might occur secondary to the decreased PA. In line with this hypothesis, our animal/cellular models in which PEPD was pharmacologically/nutritionally manipulated (HFD, CBZ-Pro or LPs-treated Mϕ) showed that when the PA was inhibited,

the PEPD release (in serum or the extracellular compartment) was increased. Conversely, in genetically manipulated mice – i.e. in both PEPD total KO and macrophage-specific KO (BMT model), the *pepd* gene had been ablated. Therefore, both PEPD activity and release are suppressed, either globally (totally in the KO and partially in the HET mice) or in the hematopoietic cells (BMT model). These designs justify why the decreased PA in PEPD genetic models is not associated with an increased release of PEPD at the systemic level. Of note, the serum level of PEPD changed in the BMT KO mice fed HFD. Collectively these data suggest that under physiological conditions, the amount of PEPD released from/by the macrophage population might be quantitatively marginal compared to the contribution of other organs/cell types. However, under pathogenic conditions -such as HFD- the expected increase in PEPD serum level was blunted suggesting that Mϕ might play a more relevant role in contributing to the elevated serum PEPD observed in obesity. We cannot completely exclude that other cells in the hematopoietic fraction might also contribute to the phenotype of the BMT KO mice, a question that will require further investigation.

The specific routes and mechanisms regulating the release of PEPD from cells still need to be defined. PEPD has been reported in several large scale profiling studies to be secreted in exosomes. [32–35]. Inflammation (e.g. obesity *in vivo* and LPS *in vitro)* could also be a possible trigger. There is some evidence supporting a role for ROS and RNS regulating the secretion of PEPD and its intracellular peptidase activity[36–38].

Our results indicate that the extracellular PEPD exacerbated fibro-inflammation and IR in obesity. However, whereas PEPD serum levels were higher in obese mice, their serum PA was not modified, suggesting that the extracellular effect was independent of the peptidase activity of PEPD. Whilst *pepd* HET, BMT KO, and CBZ-Proline-treated mice shared decreased intracellular PEPD enzymatic activity and increased fibrosis in AT, they diverged in other metabolic aspects. The CBZ-Proline-treated mice had a low residual enzymatic activity level and the highest increase in secreted PEPD, exhibiting the most severe metabolic phenotype in terms of AT fibro-inflammation and metabolic disorders. In contrast, when fed a chow diet, *pepd* HET and BMT KO mice did not exhibit increased PEPD in the serum and showed a milder metabolic phenotype. *Pepd* HET mice only showed mild metabolic dysfunction when fed HFD58%, known to promote PEPD release from the AT further. Using purified PEPD exogenously, we showed that *in vivo* and *in vitro* PEPD treatment promotes AT fibrosis and IR. Thus, we propose that “decreased PA” and “increased PEPD serum level” independently induce metabolic complications.

Our results conclude that dysregulation of PEPD elicits a dual role in mediating AT fibrosis and metabolic risk through complementary mechanisms. This conclusion was obtained by integrating the phenotypical data from murine *in vivo* models of dysregulated PEPD activity and/or secretion. This study provides a strong rationale for measuring serum PEPD in obese individuals to identify and stratify those at a higher metabolic risk by recognising their susceptibility to AT fibrosis and inflammation.

Europe PMC Funders Author Manuscripts

Methods

Human Studies

Age, BMI, and glycaemic status of the different cohorts can be found in Figure S1a.

Cohort 1 and 3—In cohort 1, we analysed 84 VsW and 70 ScW samples from Dr Josep Trueta" Hospital (Girona) participants with a wide range of adiposity (BMI between 20 and 68 kg/m^2). In cohort 3, 46 VsW and 36 ScW samples from morbidly obese subjects (BMI > 35 kg/m^2) were analysed. Subjects were Caucasian with stable body weight for three months. Subjects were studied in the post-absorptive state, had no systemic disease other than obesity, and were free of any infections in the month before the study. Specific biochemical tests excluded liver diseases (tumoral disease and HCV infection) and thyroid dysfunction. All subjects gave written informed consent, validated and approved by the ethical committee. Samples were partially provided by the FATBANK (CIBEROBN) coordinated by the IDIBGI Biobank (Biobanc IDIBGI, B.0000872), Spanish National BiobanksNetwork, processed following SOPs with approval of the Ethics, External Scientific and FATBANK Internal Scientific Committees. SAT and VAT samples were obtained from cholecystectomy, abdominal hernia, and gastric bypass surgical procedures.

Cohort 2—ScW and VsW (omental) biopsy samples were obtained from severely obese (BMI >35 kg/m^2) and lean subjects (BMI ≤25 kg/m^2) undergoing elective surgery. Obese patients candidates for bariatric surgery were studied in Paris (France) following the Helsinki Declaration and Ethics Committee of Clinical Research (CPP Ile-de-France 1, Fibrota study N° clinical trial NCT01655017). Patient phenotyping is described in[39]. Blood sampling was performed fasted one month before the surgery. The same surgeon obtained paired ScW and VscW samples. Among glucose intolerant and diabetic subjects (n=15), seven were treated with Metformin, three with insulin and two with GLP1 agonist. Exclusion criteria include anaemia, abnormal thyroid-stimulating hormone (TSH), human immunodeficiency virus (HIV) and/or hepatitis C virus (HCV) infection, severe hepatic and/or renal failure, inflammatory disorder. Signed informed consents were obtained in all lean and obese individuals agreeing with ethics regulation.

Animals

8-10 weeks old male C57Bl6/J mice were purchased from Charles River. *Pepd* KO mice were generated by the Wellcome Trust Sanger Institute Mouse Genetics Project on a C57Bl6/J background by mating heterozygous mice. *Pepd* homozygous (null and WT) and heterozygous pups were observed in normal Mendelian ratios. In respect to the 3R, only a subpopulation of the pups born was selected for each study. 8-10 weeks old male *Pepd* WT, HET and KO were used for each experiment. 8-10 weeks old male wild type and leptin-deficient mice, Lep$^{Ob/Ob}$, were on a C57BL/6 background. Details of the mouse models are provided in Table S9. This research has been regulated under the Animals (Scientific Procedures) Act 1986 Amendment Regulations 2012 following ethical review by the University of Cambridge Animal Welfare and Ethical Review Body (AWERB) under pathogen-free conditions and housed according to UK Home Office guidelines and carried out in the Disease Model Core unit. Animals were housed 3–4 per cage in a temperature-

controlled room (22°C) with a 12-h light/dark cycle, with 55% relative humidity and ad-libitum access to food and water. A standard chow diet (DS-105, Safe Diets) was administered to all animals from weaning, consisting of 64.3% carbohydrate, 22.4% protein and 13.3% lipid of total calories. Only male mice were used for *in vivo* experiments, isolation of primary cells (i.e. adipose cells, HSCs, muscle fibroblasts) and preparation of BMDMs.

Generation of Bone Marrow Chimeras

C57BLl6/J mice at ten weeks of age received a sub-lethal dose of whole-body irradiation (9 Gy). The day after irradiation, donor *pepd* KO mice were culled, and their femurs and tibias were removed aseptically. Marrow cavities were flushed in RPMI medium, and single-cell suspensions were prepared. The irradiated recipients received 1×10^7 bone marrow cells in 0.1 ml of PBS by tail vein injection. During four weeks after BMT, Bactrim (Roche) was added to drinking water. After two additional weeks, mice were switched to HFD 58%. Mice were culled 16 weeks later to collect blood and tissues.

Diets and Pharmacological challenges

Diets—Diets for animal studies included standard chow (10% calories from lipid), HFD 45% (D12451, Research Diets, 45% calories from lipid) and HFD 58% (D12331, Research Diets, 58% calories from lipid). Standard chow or HFD was provided ad libitum to animals from 8weeks old until indicated.

Insulin injection—8-10 weeks old WT, *pepd* HET and *pepd* KO male mice were injected intraperitoneally with saline solution or insulin (2U/kg) for 15 min.

Pharmacological inhibition of PEPD—8 weeks-old C57BLl6/J male mice were first fed with chow or HFD 58% for 10 weeks. CBZ-Pro supplemented pellets (both chow and HFD 58%) were prepared daily by spraying and mixing a solution of CBZ-Proline (2mM) dissolved in 70% ethanol. Mice consumed an approximatively daily dose of 60mg/kg of CBZ-Proline, a dose previously used in other murine studies[19], treatment lasted for 6 weeks, control mice were offered regular pellets. CBZ-Proline does not alter viability or promote toxic effects in mice [19]. ICBZ-Pro-treated mice did not show evidence of hepatotoxicity/ liver damage (alanine (ALAT) or aspartate (ASAT) transaminase levels) (Extended data Figure 2a).

PEPD treatment—8-10 weeks-old C57Bl/6N male mice were injected i.p. with the purified PEPD protein (0.2 mg/kg) or saline three times a week for 6 weeks[40]. Insulin and glucose tolerance tests were performed at weeks 4 and 5. PEPD treatment did not modify the ASAT levels (Extended data Figure 7e).

Body Composition

Fat and lean masses were calculated by time-domain nuclear magnetic resonance (TD-NMR) using a minispec Live Mice Analyzer LF50 (Bruker).

Glucose and Insulin Tolerance Tests

For the glucose tolerance test, mice were fasted overnight (16h) with free access to drinking water. Glucose was administered intraperitoneally (2 g/kg), and blood glucose levels were monitored from the tip of the tail with a glucometer. For insulin tolerance tests, insulin was administered intraperitoneally (0.75mU/g), and blood glucose was measured at various times after injection.

Serum Biochemistry

Triglycerides and transaminases were measured on the Dimension RXL analyser (Siemens Healthcare) or Perkin Elmer DELFIA using reagents and calibrators (Siemens). Free fatty acids were measured using the Roche Free Fatty Acid Kit (half-micro test) (kit code 11383175001). Insulin was measured using electrochemical luminescence immunoassay on the MesoScale Discovery immunoassay platform.

Explants for conditioned medium

Approximately 100 mg of freshly dissected BAT, ScW, GnW and liver pieces from 30-week-old mice in chow and HFD conditions, or VsW from human subjects cut into fine pieces were incubated for 6h hour at 37oC in 5% CO2 in DMEM with 5% heat-inactivated FBS, 20 mM HEPES, 100 units/mL penicillin, 100 μg/mL streptomycin, and 20 mM L-glutamine) (1 mL media per 100 mg of tissue).

Magnetic-activated cell sorting

GnW from 10-12 weeks old C57BL/6 mice were dissociated by collagenase treatment isolating unilocular adipocytes from the stromavascular fraction (SVF). SVF was resuspended in MACS buffer (PBS, 2mM EDTA (sterile), 0.5% Bovine Serum Albumin) and incubated with Microbeads conjugated to monoclonal antihuman/mouse CD11b (Mac-1α) antibodies (isotype: rat IgG2b, dilution 1/10, Miltenyi Biotech, 130-049-601). $Cd11^+$ fractions were isolated using MACS LS columns according to manufacturer instructions (Miltenyi Biotech).

Bone marrow-derived Mϕ preparation and treatments

Femur and tibia bones from 10-16 weeks-old C57BL6 mice or *pepd* WT, HET and KO mice were isolated and cleaned, and 10 mL of RPMI-1640 was flushed through each bone. Total bone-marrow cells were passed into a 100 μm cell strainer and counted using Countess II automated cell counter(Thermofisher). Cells were spun (400g, 5 min.), resuspended in BMDM culture medium: RPMI1640 supplemented with 20% of L929-conditioned cell medium, 10% heat-inactivated foetal bovine serum (HI-FBS), and 1% penicillin and streptomycin). To make L929-conditioned cell medium, L929 cells (CCL-1, ATCC) were seeded in DMEM supplemented with 10% heat-inactivated FBS, 100 U/ml penicillin-streptomycin and 2 mM L-glutamine (Sigma) at a density of 250,000 cells per 50 ml of medium per T175 tissue culture flask. The medium was harvested after 1 week of culture, and then 50 mL of fresh DMEM supplemented with 10% heat-inactivated FBS, 100 U/ml penicillin-streptomycin and 2 mM L-glutamine was added onto cells and harvested 1

week later. Batches obtained after the first and second weeks of culture were mixed at a 1:1 ratio, aliquoted and stored at -20 °C.

Total bone-marrow cells were seeded in 10 cm non-culture treated plates (Falcon) at a density of $5x10^6$ cells per plate per 10 ml of Mϕ differentiation medium and cultured for 7 days at 37 °C in 5% CO2. On day 5 of differentiation, the medium was removed and replaced with 10 ml of fresh BMDM culture medium. On day 7, BMDMs were detached using ice-cold PBS-EDTA 1mM, spun (400xg, 5 min.) and resuspended in fresh BMDM culture medium. Differentiated BMDMs were counted using Countess II automated cell counter, and cell concentration adjusted to 5x105 cells/ml. Immediately after, cells were plated for experiments at the following densities: 100µl/well of 96-well plate, 500 µl/well of 24-well plate, 1 ml/well of 12-well plate, 2 ml/well of 6-well plate and 10 ml per 10 cm plate. Cells were incubated for 16-24 h after plating before conducting experiments.

Mϕ purity was routinely tested by the expression of CD11b and F4/80 by flow cytometry. 93-97% of the cells express high CD11b and F4/80 after 7 days of differentiation.

After differentiation, BMDMs were cultured in 12 well-culture plate ($5 X 10^5$ cell) for 24h in BMDM medium before 6-24h stimulation with LPS (100ng/mL), DEX (100nM), IL4 (10ng/mL), purified PEPD (250nM), Gly-Pro (10mM) or CBZ-Pro (6mM) and stored -80 C prior RNA extraction or prolidase assay. Erlotinib (5µM) was added to the culture medium 2h before and during the treatment with PEPD. We validated PEPD specific effect by measuring *cox2* expression in BMDMs, reported as a PEPD target gene[15]. In addition, we discarded the potential cytotoxic effects of purified PEPD on BMDMs and its potential endotoxin contamination by boiling the purified protein and tested it on BMDMs for *cox2* induction (Extended data Figure 7a-c).

Cell Culture

RAW264.7 macrophage culture and transfection—RAW264.7 cells (TIB-71, ATCC) were cultured in DMEM (4.5g/L glucose) supplemented with 10% HI-FBS, 100 U/ml penicillin-streptomycin and 2 mM L-glutamine (Sigma). 100,000 cells per well were seeded in a 24-well plate for knockdown experiments. The following day cells were transfected using Lipofectamine™ LTX Reagent with PLUS™ (Invitrogen, ThermoFisher) according to manufacturer instructions. ON-TARGET plus siRNA against EGFR or CTR were obtained from Dharmacon (Horizon). 24h post-transfection, RAW264.7 cells were treated 24h with purified PEPD 250nM. Erlotinib (5µM) was added to the culture medium 2h before and during the treatment with PEPD.

3T3-L1 adipocytes—3T3L1 Cells were differentiated into adipocytes (day 9) accordingly to the protocol described by Roberts *et al.* [41].

Primary adipose cells—GnW from 10 weeks-old *pepd* WT, HET, KO mice was dissociated by collagenase treatment isolating unilocular adipocytes from the stromavascular fraction (SVF). Floating adipocytes were collected and used for lipolysis assay (on the day of isolation) or culture in hydrogel $48h^6$ to measure Il-6 secretion in response to purified

Europe PMC Funders Author Manuscripts

PEPD. Preadipocytes were isolated from the SVF and differentiated into adipocytes (day 9) accordingly to the protocol described by Lacasa *et al.*[42].

Primary HSCs—Hepatic stellate cells (HSCs) were isolated from livers of 10-12 weeks-old C57Bl/6 mice. Liver tissue was digested with pronase and collagenase B (Roche), and the cell suspension was subsequently separated by an 11.5% Optiprep gradient (Sigma). HSCs were cultured into plastic (Corning) using DMEM supplemented with pyruvate (1%), glutamine (1%), penicillin-streptomycin (1%) and HI- FBS (during the activation process: 16%; in fully activated HSCs: 10%); all reagents were from Life Technologies. HSCs were grown at a confluence of 35,000 cells per cm^2 on Corning well 6 plates (RNA) or (for immunofluorescence, IF) in Nunc Lab-Tek Permanox plastic Chamber Slide System (Sigma, C7182-1PAK). HSCs were treated with purified PEPD (250nM) 24h (RNA) or 5 days (IF).

Primary muscle fibroblasts—Both hind limbs from 10-12 weeks-old C57Bl/6 mice were removed by dislocating hip joints and were dissected in 5 ml digestion medium (Collagenase II 30mg, Dispase II 36mg, 1M HEPES 2.5%, DMEM high glucose, P/S 1%, 15ml). Enzymatic digestion was carried on for 20 minutes in a 37°C shaking bath and stopped with DMEM 20% FBS. Sequentially, the cell mixture was passed through 100 μm, 70 μm, and 40 μm cell strainers and pelleted at 400 x g for 5 min at room temperature. Cells were resuspended in 12 ml seeding medium (Ham F12, 20% FBS, 10% horse serum (HS), 1% L-glutamine, 1% pen/strep, and 10ng/ml basic fibroblast growth factor (FGFb) and plated on an uncoated 10-cm petri dish for one hour at 37°C, 5% CO_2. The medium was changed for fresh seeding medium and renewed every two days until reaching 70% confluence. Fibroblasts were grown at a confluence of 50,000 cells/wells in 12 well plates (for RNA) or 25,000 cells/well in 24 well plates (on coverslips, for IF). Fibroblasts were pre-treated or not with Erlotinib (5μM) prior to treatment with purified PEPD protein (250nM) for 24h (RNA) or 5 days (IF).

Lipolysis Assays

Primary mature adipocytes were isolated from GnW of C57Bl/6mice and incubated in Krebs–Ringer bicarbonate buffer with an increasing dose of NE (10^{-10}-10^{-5} M) for 2 h at 37°C. Glycerol was measured as an index of lipolysis by using free glycerol reagent (Sigma) against a glycerol standard curve.

Prolidase activity

PA was determined optimising Myara's spectrophotometric procedure, modified from the Chinard technique[43,44] and miniaturised in 96 acid-resistant well plates. Briefly, Tissue and Mϕ cell extracts were mixed V/V with PBS 50 mM HEPES/1mM MnCl2 and 0.75 mM GSH and incubated 20 min at 50 C. The activated mixture was then added V/V to PBS 94 mM glycyl-proline (Gly-Pro) for a final concentration of 47 mM and incubated or not (control corresponding to basal levels of proline in the cell/tissue extracts) 60 min at 37°C. The reaction was stopped by adding 6V of 0.45 M trichloroacetic acid and centrifuged at 4300 rpm for 60 min. The supernatant (1V) was then added to 4V of a 1:1 mixture of glacial acetic acid and Chinard's reagent (25 g of ninhydrin dissolved at 70 °C in 600 ml of glacial acetic acid and 400 ml of 6 M orthophosphoric acid) and incubated 15-45 min

at 90 C. Absorbance was read at 515nm, and proline concentration was calculated using proline standards ranged from 0.5 μg to 32 μg. Enzyme activity was reported in micromole of proline released per minute per milligram of protein.

GC-MS analysis of amino acids

Plasma and GnW explants samples were analysed for free amino acid concentrations using the EZ:fast GC-MS Kit (KGO-7166 Phenomenex Inc., Torrance, CA, USA).

Extraction—AT (~100 mg) was weighed and amino acids were extracted into 1ML of 75% 0.01M HCL and 25% acetonitrile using a FastPrep (MP Biomedical). All liquid was removed to 1.5 ml Eppendorf tube and centrifuged at 16,000 g for 10 min. Following centrifugation the upper lipid layer was discarded and the lower ACN/aqueous layer was removed to a fresh Eppendorf tube and the centrifugation step was repeated. Samples were transferred to another fresh Eppendorf tube and dried overnight using a speedvac before being resuspended in 100 μl of 0.9% saline by repeatedly pipetting up and down and vortexing (3x) for 5 seconds. After resuspension, samples were centrifuged at max speed for a further 10 min. and analysed following the EZ-faast protocol.

Modified EZ-FAAST Protocol—Amino acids were analysed using the EZ:faast free (physiological) amino acid analysis kit (KGO-7166) for GC-MS according to manufacturer's instructions up to the chromatography step. Briefly, 100 μl of serum or WAT extract was mixed with 100 μl of reagent 1, which contained 0.2 mM Norvaline as an internal standard. Samples were drawn into the propriety sorbent tip and then washed by drawing a further 200 μl of reagent 2 followed by air through the tip until dry. Samples were eluted by attaching a new syringe to the tip, drawing the eluting medium (200 μl total) into the tip until the sorbent granules were wet then ejecting the granules. Samples were then derivatised by adding 50 μl of reagent 4 using a Drummond Dialamatic Microdispenser and vortexing for 5-8 seconds. Samples were allowed to stand for 1 minute, then vortexed again and allowed to stand for a further minute. 100 μl of reagent 5 was added and samples were vortexed for 5 seconds and allowed to stand for 1 minute. The upper layer was transferred to an autosampler vial and dried under nitrogen for 10 min.. Samples were resuspended in 100 μl of reagent 6 and transferred into an insert in the same autosampler vial. Samples now proceeded to chromatography.

Chromatography—Gas-Chromatography Mass spectrometry analysis was performed using an Aglient 7890B GC and an Agilent 5977A MSD using a 0.25 mm ID, 0.25 μM film thickness x 15 M DB-1701 (Cat: 122-0712, Agilent) column. The GC-Conditions were as follows:

Inlet conditions: Inlet temperature: 250°C ; Split 10:1 for serum, splitless for Gly-Pro determination and adipose tissue; Inlet liner Liner, Phenomenex AG0-4680: 900 μL (FocusLiner) – part of kit ; Column Flow 2 ml/min ; Injection volume – 1μl

Temperature Program: 75°C Hold for 2 minute; 16.3°C/min until 280oC; 280°C Hold for 5.5 min.; MSD transfer line 280°C

Europe PMC Funders Author Manuscripts

MSD conditions: Scan 45-450, 4 Hz; MS Source temperature 240°C; MS Quad temperature 180°C. Data was acquired using MassHunter Workstation Software.

Peak integration and quantification was performed using MassHunter Workstation Quantitative Analysis software (version B.07.00, Agilent) selecting ions for each amino acid specified in EZ:faast protocol. Data was analysed by first normalising all data points to the Norvaline internal standard. Amino acid concentrations were then determined using a 3 point standard curve made using 25, 50 and 100 µl of the 0.2 mM standards provided in the EZ:faast kit. AT extracts and serum were expressed as nMoles per 100µl of sample.

Histological Analysis

AT and liver samples were fixed in 4% paraformaldehyde for 24h, embedded in paraffin, sectioned into 5 µm sections, and processed for Sirius (fibrosis) or haematoxylin and eosin (H&E) (liver steatosis) staining. The slides were scanned (Microscopy Zeiss Axioscan Z1 Slidescanner) and processed for fibrosis (Sirius staining excluding vessels) and steatosis (Vacuole % area) quantification using HALO™ Image Analysis Software (HALO; Indica Labs).

Confocal Analysis

Cells were fixed in 4% paraformaldehyde for 1 hour at room temperature, then transferred to PBS, and stored at 4 °C until immunofluorescence analysis. Samples were blocked in 1M glycine and PBS with 3% BSA and 0.1% Triton X-100 and then incubated overnight (4 °C, in agitation) with primary antibody diluted in blocking buffer (PBS 3% Albumin, PH=7.4). Antibodies used were anti-αSMA 1A4 (1:200, Sigma, A2547) and anti-collagen I (1:200, Abcam, ab21286). After washing in PBS and blocking, cells were incubated with the secondary antibodies conjugated to Alexa Fluor® dyes, either Alexa555-conjugated anti-rabbit (1/250, Life technologies, A21428) or Alexa488-conjugated anti-mouse (1/250, Life technologies, A21202), BODIPY 493/503 (1/2000, Life science, D-3922), used as a stain for neutral lipids, and Phalloidin-iFluor 594 (1/200, Abcam, ab176757) used to stain the actin filaments, for 1h at RT in blocking buffer, followed by Hoechst 33342 (1/2000, Thermofisher, H3570) for 5 min, and multiple PBS washes. Samples were mounted and imaged blind using Zeiss LSM 510 Meta Confocal microscope with LSM 3D software (Carl Zeiss). At least three images per sample per stain were used for quantification performed blind. Staining quantification was performed using Fiji software (https://imagej.net/software/fiji/). A detailed list of the antibodies used for this study is presented in Table S9.

Hydroxyproline Assay

Hydroxyproline measurement was done using a hydroxyproline colorimetric assay (BioVision) as previously described[45]. Briefly, frozen fat is weighted and heated in 6 N HCl at 110°C overnight in sealed tubes, as 10 µL of HCl/mg of WAT. Ten microliters are evaporated before incubation with chloramine-T and p-di-methyl-amino-benzaldehyde (DMAB) at 60°C for 90 min. The absorbance was read at 560 nm, and the concentration was determined using the standard curve created with hydroxyproline.

Europe PMC Funders Author Manuscripts

ELISA assays

Murine and human PEPD protein concentration was measured using respectively an ELISA kit for Mouse Xaa-Pro dipeptidase (PEPD) ELISA kit (CSB-EL017784MO, CUSABIO) and Human PEPD (Peptidase D) ELISA Kit (E-EL-H5575.96, Elabscience) in tissue explants (from which debris was removed by centrifugation) and serum according to the manufacturer's instructions. Leptin protein concentration in AT explant media was measured using an ELISA kit for murine Leptin (R&D systems, DY498). IL-6 protein concentration in conditioned media from mature adipocytes isolated from GnW was measured using an ELISA kit for murine IL-6 (R&D systems, DY406). A standard curve was prepared according to the manufacturer's instructions, and the value associated with an unconditioned media blank was subtracted from that of conditioned media.

RNA Extraction and Real-Time PCR

RNA from cells extracted using RNeasy Mini columns (Qiagen) according to the manufacturer's instructions. RNA was harvested from frozen tissue using RNA-STAT-60TM (AMS Bio) and purified by chloroform extraction and isopropanol precipitation. Reverse transcription was performed using Reverse Transcriptase System (Promega) according to the manufacturer's instructions. Real-time PCR was carried out using TaqMan or Sybr Green reagents using an Abi 7900 real-time PCR machine using default thermal cycler conditions. Primer sequences are described in Table S9. Reactions were run in duplicate, checked for reproducibility, and then averaged. A standard curve generated from a pool of all cDNA samples was used for quantification. The expression of genes of interest was normalised using the geometric average of four housekeeping genes (18s, 36b4, βactin, and B2m), and data are expressed as arbitrary units.

Regarding human samples (Cohorts 1, 2, 3), RNA purification, gene expression procedures and analyses were performed, as previously described [46,47]. Total RNA was briefly extracted and purified using RNeasy Lipid Tissue Mini kit, and Agilent Bioanalyzer checked the integrity. Total RNA was quantified using a spectrophotometer. The same amount of total RNA was reverse transcribed to cDNA from all samples using a High-Capacity cDNA Archive kit following manufacturers' instructions. Gene expression was assessed using a LightCycler 480 real-time PCR system, using TaqMan and SYBRgreen technology suitable for relative gene expression quantification. The commercially available and pre-validated TaqMan primer/probe sets used are described Table S9 and S10.

RNA sequencing

Library preparation and sequencing—Total RNA of GnW and liver was extracted using the miRNeasy mini kit (Qiagen) according to the manufacturer's instructions. Per experiment, 4-10 independent biological repeats were used.

Total RNA was quality checked (RIN >7) via the Agilent Bioanalyser 2100 system, using the Agilent RNA 6000 Nano Kit. 1ug of RNA was used to construct barcoded sequencing libraries with the TruSeq Stranded mRNA HT Sample Prep Kit (Illumina) following the supplier's instruction. All the libraries were validated using the Agilent Bioanalyser DNA

12000 and then multiplexed and sequenced on two lanes of Illumina HiSeq 4000 at SE50 at CR-UK Cambridge Institute Genomics Core Facility.

Processing of RNA-Seq data—RNA-Seq reads (Table S1) were mapped to the most recent ENSEMBLE version GRCm38.p5 of the mouse reference genome sequence (GRCm38.p5) using STAR v2.5.1b[48] including the annotations as hints for exon-intron borders. Reads were considered mapped if the similarity was at least 95% over at least 90% of the read length as previously described[49]. FeatureCounts v1.5[50] was applied for the generation of count tables based on the mapping files. Customised python scripts[49] were deployed for downstream processing, including the raw counts' normalisation to the total number of assigned reads per gene (TPMs) and the combined exon length (FPKMs), respectively.

Gene expression and pathway enrichment analyses—Raw counts were subjected to differential gene expression analysis via DESeq2[51] and different R packages (Supplementary software). Genes, which showed raw counts lower or equal to 2 in 50 % of all samples, were removed before the differentially expressed analysis. Wald test was applied to extract differentially expressed genes (DEGs, Table S2, S3, S6-S8). Obtained DEGs were annotated via customised python scripts. Pathway enrichment analyses were performed with PIANO[52], using the gene set collection C2 retrieved from the Molecular Signatures Database (MSigDB)[53,54] (Table S4, S5). Bonferroni and Holm method was applied to correct for multiple testing.

Western Blotting

Proteins were extracted from tissue in lysis buffer (20 mM Tris-HCl, 150 mM NaCl, 1 mM EDTA, 1 mM EDTA, 1% Triton X-100, pH 7.5) with added protease inhibitor (Roche) and phosphatase inhibitor (Roche) cocktails. Debris and fat were cleared from lysates by centrifugation. Protein concentration was determined by Dc Protein assay (Bio-Rad). After dilution in Laemmli buffer with 0.5% 2-mercaptoethanol, 30 μg protein was loaded per well and subjected to SDS-PAGE in a 4%–12% gradient gel using the Novex NuPage midi system (Life Technologies) and transferred using the iBlot transfer system and reagents (Life Technologies). Membranes were blocked for 1 hour in 3% BSA in tris-buffered saline at room temperature and incubated overnight at 4oC with the following primary antibodies: anti- PEPD (1/1000, Abcam, ab86507), anti-phospho-NF-κB p65 (Ser536) (1/1000, clone 93H1, Cell signalling, #3033), anti-NF-κB p65 (1/1000, Cell signalling, #3034), anti-β-Actin (1/2000, Abcam, ab8227), anti-GADPH (1/1000, Cell signalling, #97166S), anti-β-Tubulin (1/1000, Cell signalling, #2146S), anti-phospho-AKT (Ser473) (D9E) (1/1000, Cell Signalling, #4060), anti-AKT (1/1000, #9272). Bound primary antibodies were detected using peroxidase-coupled secondary anti-rabbit (1/10 000, #7074, Cell signalling) or anti-mouse (1/10 000, #7076, Cell Signalling) and enhanced chemiluminescence (WBLUF0500, Millipore). Blots were exposed digitally using the ChemiDoc MP System (Bio-Rad), and bands were quantified using Fiji software (https://imagej.net/software/fiji/). The expression of proteins was normalised to protein levels of a housekeeping protein (β-actin, GADPH or β-tubulin), and the phosphorylation status was determined by normalising to a respective

total protein. All protein quantification data is expressed as arbitrary units. A detailed list of the antibodies used for this study is presented in Table S9.

Array-based detection of phosphorylated receptor tyrosine kinase

The Proteome Profiler Mouse Phospho-RTK Array Kit (R&D Systems, USA, Catalog Number: ARY014) was employed to screen for the phosphorylation level of receptor tyrosine kinase (RTKs) in BMDMs in response to purified PEPD, according to the manufacturer's instructions. Briefly, the array membranes were incubated 1h with an array blocking buffer before incubation overnight at 4C on an orbital shaker with 1.5 ml of cellular extract. The membrane was then washed and incubated for 30 min. with a streptavidin-HRP solution. Membranes were exposed digitally using the ChemiDoc MP System (Bio-Rad), and spots were quantified using Fiji software (https://imagej.net/software/fiji/). One condition corresponds to a pool of cellular extracts from 4 independent experiments. All the arrays were measured three times; each spot was normalised to the positive controls. The results are presented in a heat map and considered relevant when the fold variation was >1.3 or <0.6.

Cytotoxicity assays

To determine the cytotoxic effect of compounds on Mϕ, cells were seeded in Roswell Park Memorial Institute (RPMI) 1640 Medium without FBS supplemented at a density of 15,000 cells per well in wells of 96 wells plate. Cells were treated with the given compounds at the given concentrations for 24 hours, and cytotoxicity was measured using an LDH-Cytotoxicity Calorimetric Assay Kit (BioVision) according to the manufacturer's instructions.

Data Analysis

The number of animals or independent experiments was determined based on pilot data and indicated in the figure legends. No statistical methods were used to predetermine the total number of animals needed for this study. Animal allocation to cages (4 mice/cage) and diet were not randomised as we ensured each cage had mice from the three genotypes and each group (chow and HFD, control and CBZ-Pro) had the same average of initial body weight. All data from experiments are summarised by their mean and standard error. The number of replicates is reported in the figure legends. When the pairwise comparison results are expressed as a fold-change, it is declared in the figure legends to what value the data were normalised. Statistical analyses were performed using GraphPad Prism (version 8.0.2). Comparisons between two groups were conducted using an unpaired t-test. Comparison between more than two groups was conducted using a one-way ANOVA followed by appropriate post hoc multiple comparisons tests. Comparisons between more than two groups and factors were conducted using a two-way ANOVA followed by appropriate post hoc testing. Pearson's coefficients were evaluated to estimate the correlation between data series.

Data were excluded when identified as outliers using Grubbs' test (https://www.graphpad.com/quickcalcs/Grubbs1.cfm). The animals were randomly assigned to the different experimental settings (GTT, ITT). Areas under the receiver operating characteristic

Europe PMC Funders Author Manuscripts

(ROC) curves were determined for each variable to identify the predictors of AT fibro-inflammation and insulin resistance/type 2 diabetes. ROC curve is a plot of sensitivity (true positive) versus 1–specificity (false positive) showing the ability of biomarker (PEPD level) to discriminate between true positives (e.g. insulin resistant) and true negatives (e.g. insulin sensitive). The best marker has a ROC curve shifted to the left with the area under the curve close to unity[55]. The Youden index was calculated (sensitivity + specificity-1) to determine the optimal cut-off values for fibro-inflammatory status or insulin resistance indices. The values for the maximum of the Youden index were considered the optimal cut-off points using the Web-tool easyROC[56].

Exploratory Factor Analysis—Exploratory factor analysis (EFA) is an unbiased statistical method, which establishes the cluster of biological variables with high loadings (correlation equivalent) on each specific factor in a reduced number of underlying variables ("factors") considered as "superfamilies" of variables[57]. EFA was conducted to determine the possible latent structure of the variables (listed, e.g., in Figure 1.p – rows of the depicted matrix) measured in each animal model, i.e., *pepd* CBZ-Pro-treated mice, BMT mice and PEPD-treated mice. Factor analysis identifies a minimum number of new variables (factors), which are linear combinations of the original (measured) ones, such that the new (fewer) variables contain most or all the information and can facilitate the interpretation of a complex multivariate scenario. First, a matrix of correlation coefficients is computed, and a set of principal components (factors) is extracted from it. The relationships between the original variables and the factors are expressed in terms of “factor loadings”, which estimate the degree of correlation between the original variables and the factors.

We determined whether our data were appropriate for EFA using the Kaiser–Meyer–Olkin (KMO) measure of sampling adequacy and Bartlett’s test of sphericity. Data were considered appropriate if the KMO was >0.7 and Bartlett’s test was significant at $P < 0.05$. To determine the number of factors to retain, we decided to rule out the components associated with eigenvalues less than 1. The parallel analysis confirmed that our choice was viable. Factors extraction was computed using the Maximum Likelihood Estimate (MLE) method, implemented in the function fa of the psych R package[58]. Plots were produced either using in house scripts or using built-in functions of the FactoMineR R package[59].

Principal components analysis—Principal components analysis of the Lukk and the own dataset were calculated in R version 3.1.2 using the *prcomp* function of the *stats* package[60].

Europe PMC Funders Author Manuscripts

Extended Data

a

Cohort	Status	N	age	BMI	Gly mmol/L	Ins µUI/L	HOMA IR	HbA1C %	CholTmmol/L	Trigly mmol/L
Cohort 1	Non obese	26	53.6±12.2	25.9±2.9	95.5 (86-104.2)					111 (81.7-152.7)
	Obese	58	**44.3±8.9****	**44.8±7.3*****	95.5 (86.2-115.7)					96.5 (78.7-136.2)
Cohort 2a	Lean	8	46.3±4	23.9±0.6						
	Obese non diabetic (ND)	8	40.5±2.5	**51.1±2.8*****						
Cohort 2b	Obese non diabetic (ND)	6	35.3±5.3	44.7±1.8	4.8±0.117	15.22±4.3	3.3±0.99	5.42±0.09	4.9±0.2	1.19±0.198
	Obese diabetic/glucose intolerant (D/GI)	2/6	36.5±5.89	46.78±2.07	5.413±0.47	22.29±5.03	5.19±1.07	**6.143±0.17****	4.61±0.28	1.214±0.135
Cohort2c	Obese	12								
Cohort 2d	Lean	10	43.9±4.3	27.4±1						
Cohort2e	Obese	9	44.4±2.3	**42.8±0.5*****	5.4±0.4	19.6±4.4	4.8±1.4	5.9±0.1	5.6±0.4	1.4±0.3
Cohort2f	Obese non diabetic (ND)	6	36.5±5	46±3.1	5.2±0.2	19.7±4.6	4.6±1.2	5.5±0.1	5.3±0.3	1.5±0.1
	Obese diabetic/glucose intolerant (D/GI)	1/6	46.9±5.5	43.7±2.6	**6.2±0.3***	14.8±1.9	3.6±0.6	**6.7±0.2*****	4.8±0.5	1.7±0.2

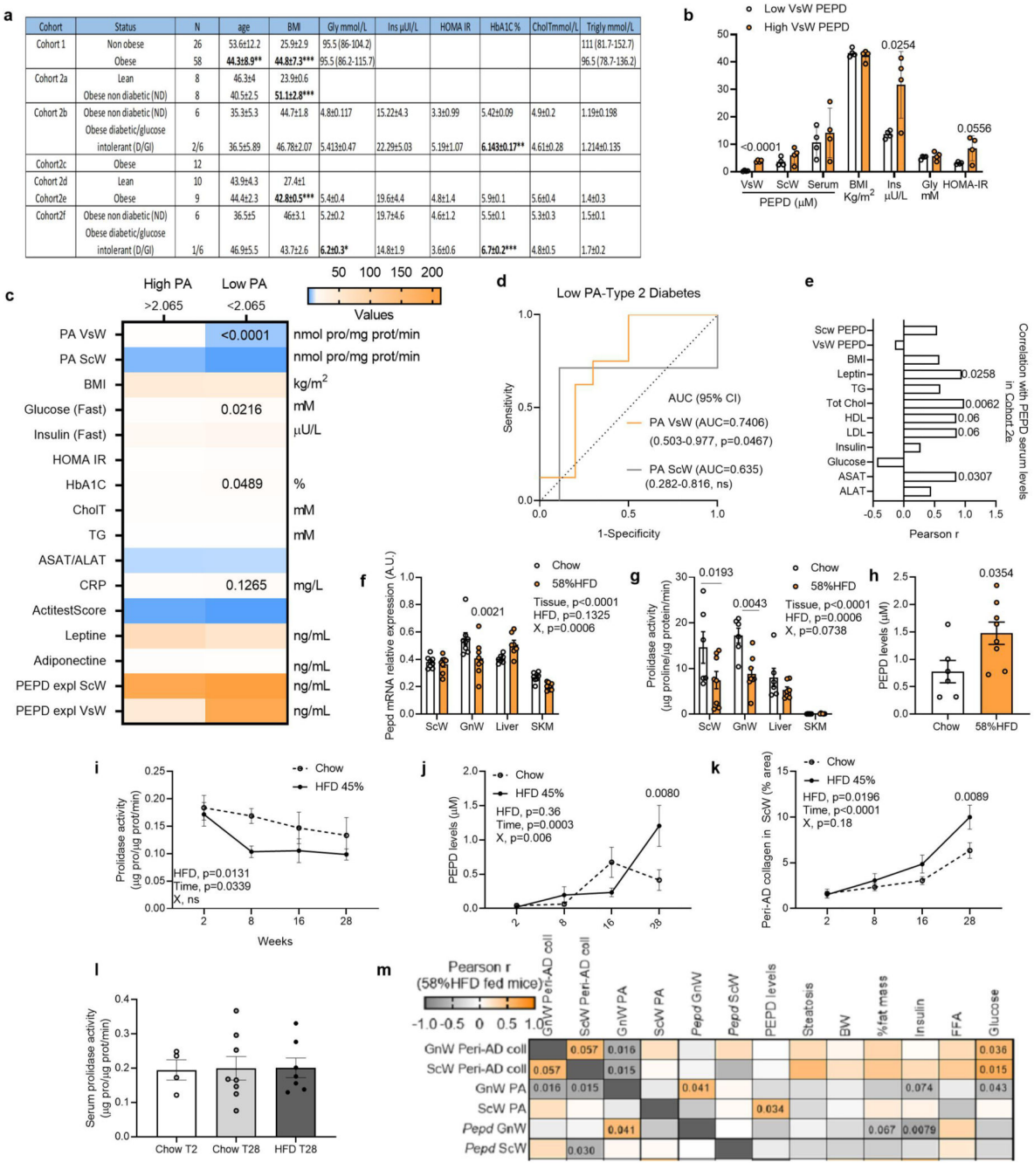

Extended Data Fig. 1. Obesity reduces AT PEPD activity and promotes PEPD release in association with AT fibrosis and insulin resistance

a, Age, BMI, glycaemic and lipidic status in the different human cohorts. **b**, PEPD serum/ScW levels, BMI and metabolic parameters in obese subjects from cohort cohort 2e (n=9) with low vs. high VsW PEPD levels. **c**, PEPD activity/ecplants levels, BMI, blood chemistry parameters and liver Actitest score in obese subjects (cohort 2e,f) with high (>2.065 nmol pro/mg prot/min) *vs.* low (<2.065 nmol pro/mg prot/min) PEPD peptidase

activity in VsW. **d**, Area under the receiver operating curve (AUC) values (95% CI) for VsW and ScW PEPD peptidase activity (PA) to discriminate subjects with type 2 diabetes (cohort 2e,f).**e**, Pearson correlation between PEPD serum levels and, ScW and VsW ECM remodelling markers and metabolic parameters in obese subjects from cohort 2b (n=14 biologically independent samples). **f, g**, Pepd mRNA relative expression (f), and PEPD prolidase activity (g) in ScW, GnW and liver from C57Bl/6 mice in chow (n=6) and 58% HFD (n=8, 20 weeks) conditions.* compared to chow diet. **h**, ELISA analysis of PEPD protein in serum from C57/Bl6 mice fed chow (n=6) or 20 weeks 58% HFD (n=8). **I-k**. ScW prolidase activity (i), PEPD serum level (j) and ScW peri-ad collagen in C57Bl/6 mice fed 2, 8, 16 or 28 weeks (n=8/group) with chow diet (ch) of HFD 45% (HF). **l**, Prolidase activity in the serum of C57Bl6 mice fed chow (2, 28 weeks) or HFD 58% (28 weeks). **m**, Pearson correlation matrix between ScW and GnW ECM remodelling markers and metabolic parameters in chow and HFD conditions (n=22). Data presented as mean values +/- SEM. Data was analysed using a two-tailed Student's *t*-test (b, c, h) or a 2-way ANOVA followed by a Sidak post-hoc multiple comparisons test (f, g, i-k).

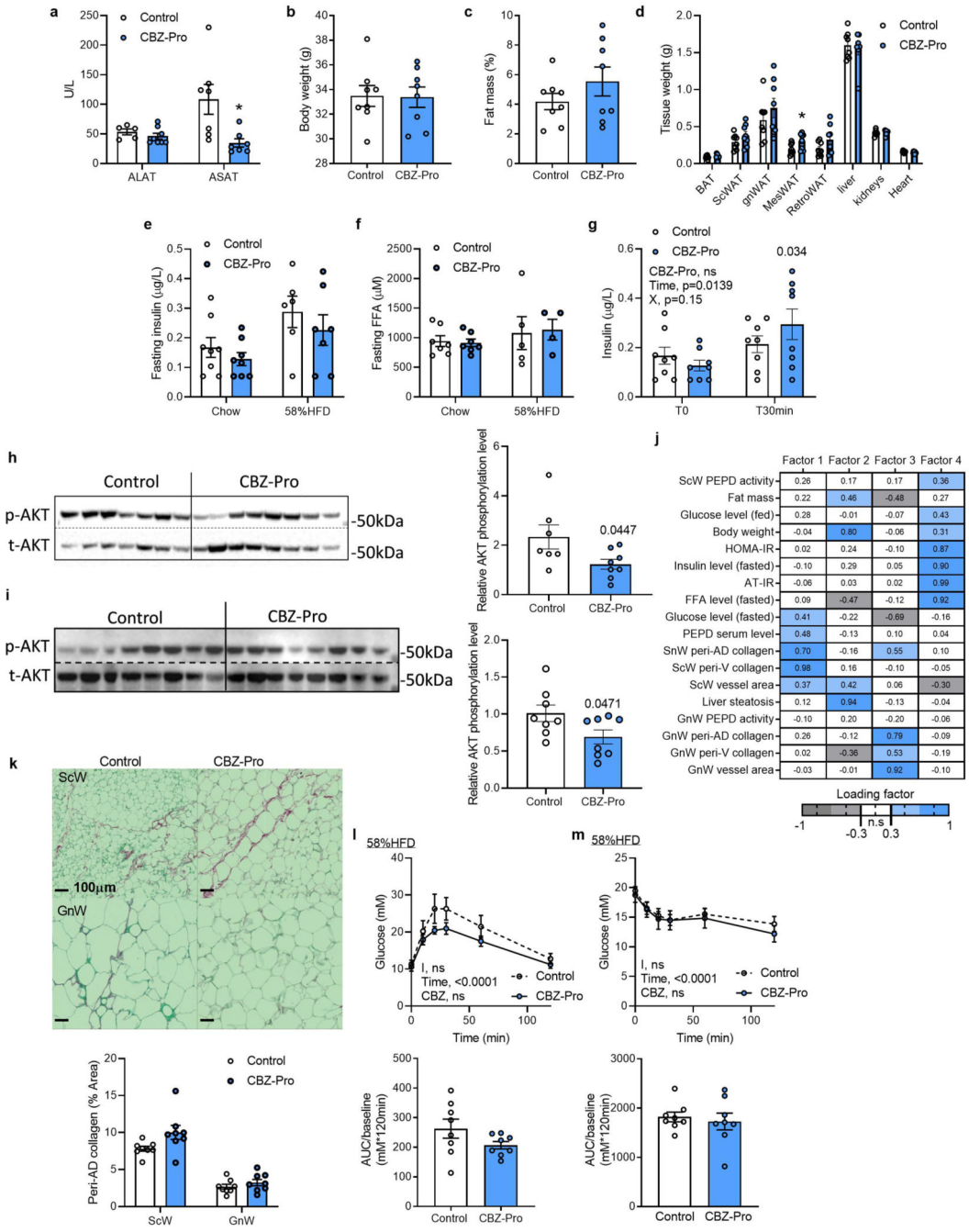

Extended Data Fig. 2. PEPD pharmacological inhibition promotes AT fibro-inflammation independently from obesity

a-d. ALAT and ASAT serum levels (a), body weight (b), and fat mass % (c), and tissue weight (d) in mice treated 10 weeks or not (control) with CBZ-Pro (n=8 biologically independent animals per group). **e, f**. Fasting insulin and FFA blood levels from CBZ-Pro-treated mice compared to control mice (n=8 biologically independent animals per group) fed chow and HFD 58% for 16 weeks. **g**. Fasting insulin blood level before and 30min after glucose injection (2g/kg) in CBZ-Pro-treated mice compared to controls

Europe PMC Funders Author Manuscripts

(n=8 biologically independent animals per group). **h,i**. Representative images of blots and quantification of total and basal phosphorylated (Ser473) AKT in GnW (h) and gastrocnemius muscle (i) of CBZ-Pro- treated mice compared to controls (n=8 biologically independent animals per group). **j**. Heat map representing the four factors extracted through exploratory factor analysis. The columns report the factors loadings of the observed variables. **k**. Representative images of red Sirius staining in ScW and GnW of control and CBZ-Pro treated mice (n=8 biologically independent animals per group) fed HFD 58%, and corresponding quantification of peri-adipocyte collagen content (peri-AD) represented in % Area (excluding perivascular staining). **l, m**. Blood glucose levels up to 120 min. after an intraperitoneal injection of glucose (2g/kg) in a glucose tolerance test (l) or insulin (0.75 IU/kg) in an insulin tolerance test (m) in control and CBZ-Pro treated mice (n=8 biologically independent animals per group) fed HFD 58%. Respective AUC are represented. Data is presented as mean values +/- SEM. Data was analysed using a two-tailed Student's *t*-test (a-d, h, i l, m) or a 2-way ANOVA followed by a Turkey (e-g) or Sidak (k-m) post-hoc multiple comparisons test.

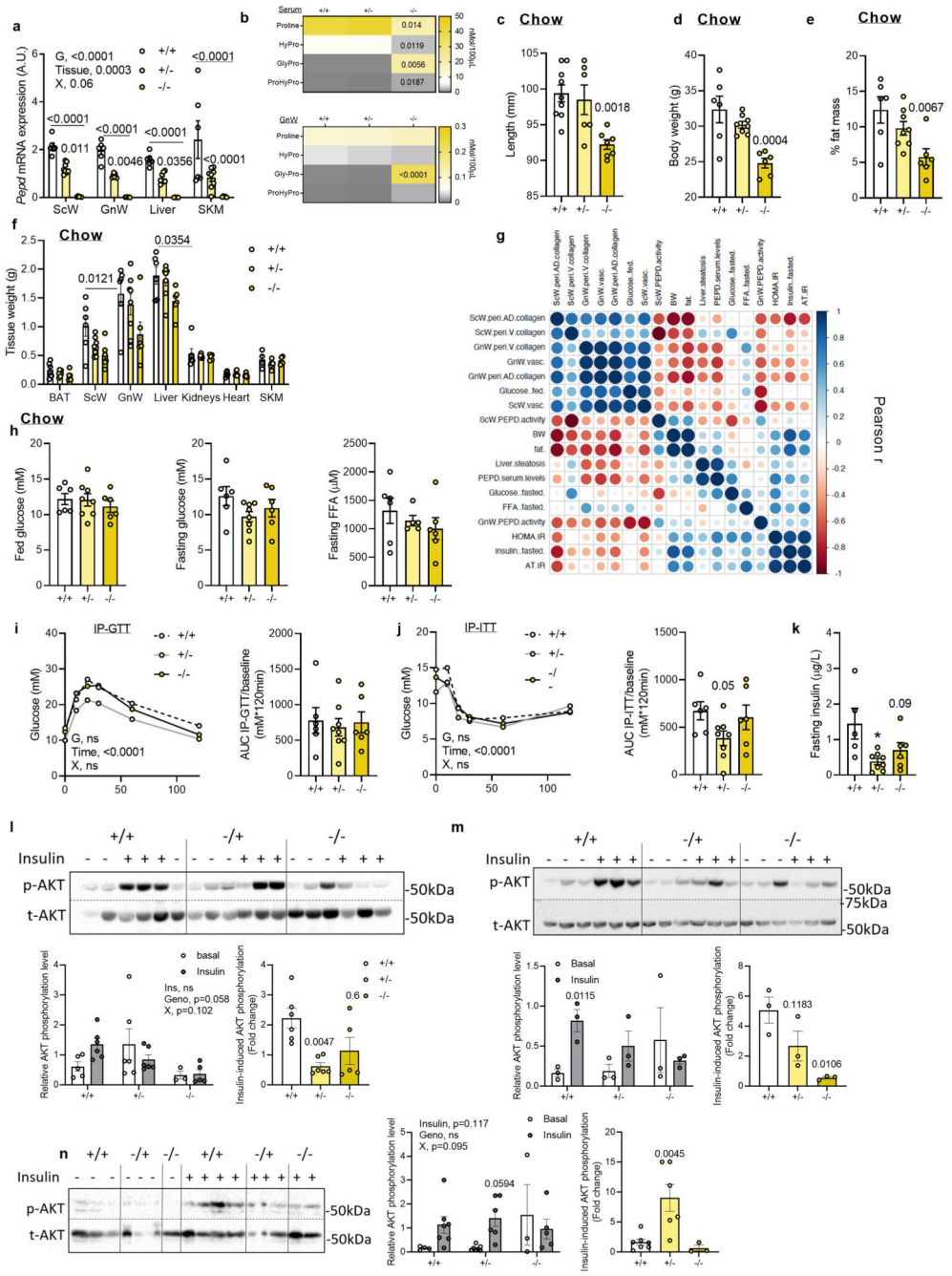

Extended Data Fig. 3. *Pepd* silencing promotes AT fibrosis but does not affect metabolic parameters in chow fed mice.

a. *Pepd* RNA relative expression in ScW, GnW, liver and gastrocnemius (SKM) from *pepd* WT (n=6), HET (n=8) and KO mice (n=5). **b**. Level of amino acids related to proline metabolism in the serum or GnW explant medium from *pepd* WT (n=6), HET (n=8) and KO mice (n=5). **c-f, h, k**. Body length (c), body weight (d), fat mass % (e), tissue weight (f), fed glucose, fasting glucose and FFA (blood levels h), and fasting insulin blood level (k) in *pepd* WT (n=6), HET (n=8) and KO (n=5) mice fed chow diet. **g**. Pearson correlations matrix

Europe PMC Funders Author Manuscripts

between ScW and GnW ECM remodelling markers, PEPD serum levels and metabolic parameters in *pepd* mice fed chow (n=19 biologically independent samples). **i, j**. Blood glucose levels up to 120 minutes after an intraperitoneal injection of glucose (2g/kg) in a glucose tolerance test (i, IP-GTT) or insulin (0.75 IU/kg) in an insulin tolerance test (j, IP-ITT), and respective AUC adjusted to basal, in *pepd* WT (n=6), HET (n=8) and KO (n=5)mice fed chow diet. **l-n**. Representative images of blots and quantification of total and phosphorylated (Ser473) AKT in GnW (l), liver (m) and gastrocnemius (n) of pepd WT (n=6-11), HET (n=6-12) and KO n=6-8) mice fed chow diet after i.p injection of saline or insulin. 2way ANOVA with Dunnett's (a) or Sidak's (I, k, l-n) post-hoc multiple comparisons test; G, genotype; X, interaction. Data is presented as mean values +/- SEM. Data was analysed using a One way ANOVA followed by a Dunnett (b-f, h, k) or Sidak (i, j, l-n) post-hoc multiple comparisons test.

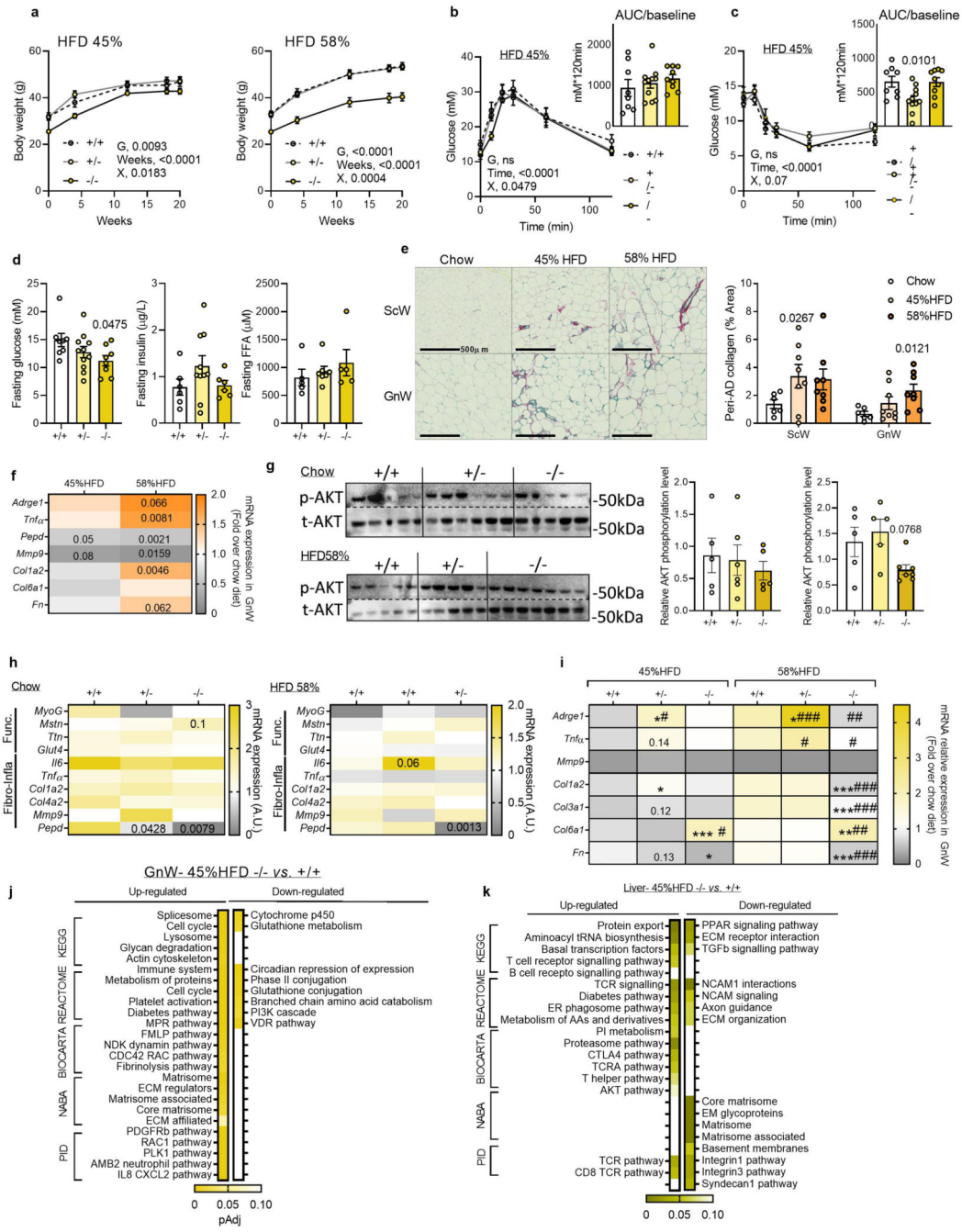

Extended Data Fig. 4. *Pepd* silencing exacerbates metabolic disturbances in HFD 58%-fed mice. Body weight curves and fat mass % curves of *pepd* WT, HET and KO mice after 20 weeks HFD 45% (n=8, 11, 9 biologically independent animals per group, respectively) and HFD 58% (n=8, 11, 8 biologically independent animals per group, respectively). **b, c**. Blood glucose levels up to 120 min. after an intraperitoneal injection of glucose in a glucose tolerance test (b) or insulin (0.75 IU/kg) in an insulin tolerance test (c) with the representative AUC in *pepd* WT (n=9), HET (n-11) and KO (n=9) mice fed HFD 45%. **d**. Fasting glucose, insulin and FFA blood levels in *pepd* WT (n=8), HET (n=11) and KO

Europe PMC Funders Author Manuscripts

(n=8) mice fed HFD 45%. **e**. Representative images of red Sirius staining in ScW and GnW from C57Bl/6 mice fed chow (n=6), 45%HFD (n=8) and HFD 58% (n=8, 20 weeks) conditions and quantification of peri-adipocyte collagen content (peri-AD) represented in % Area (excluding perivascular staining).**f**. Heat map of gene expression in GnW from C57Bl/6 mice fed 20 weeks with chow (n=6), 45%HFD (n=8) and HFD 58% (n=8). Results are expressed as fold change over chow diet. **g**. Representative images of blots and quantification of total and basal phosphorylated (Ser473) AKT in gastrocnemius muscle of pepd WT, HET and KO mice fed chow (n=5, 6, 5 biologically independent animals per group, respectively), and HFD 58% conditions (n= 5, 5, 7 biologically independent animals per group, respectively). **h**. Heat map of gene expression of fibro-inflammatory and functional markers in gastrocnemius of *pepd* WT, HET and KO mice fed chow (n=6, 7, 6 biologically independent animals per group, respectively), and HFD 58% conditions (n= 8, 7, 8 biologically independent animals per group, respectively). **i**. Heat map of gene expression in GnW from *pepd* WT, HET and KO fed HFD 45% (n=6, 10, 9 biologically independent animals per group, respectively) and HFD 58% (n=8, 9, 9 biologically independent animals per group, respectively) expressed as fold change variation over chow diet; *p<0.05 compared to chow, #p<0.05 compared to WT. **j, k**. Pathway enrichment analysis of the DEGs in GnW (i) and liver (j) from *pepd* KO mice (n=9) compared to WT mice (n=8) fed HFD 45%, using different data bases (KEGG, Reactome, Biocarta, NABA and PID). The heat maps indicate the level of significant changes (false discovery rate-adjusted p-value). Data is presented as mean values +/- SEM. Data was analysed using a 2-way ANOVA followed by a Turkey post-hoc multiple comparisons test; G, genotype; X, interaction (a-c, **i**), or a one way ANOVA followed by a Sidak (b, c, e) or Dunnett (d, g, h) post-hoc multiple comparisons test. A two-tailed Student's *t*-test was also used to analyse the data (f).

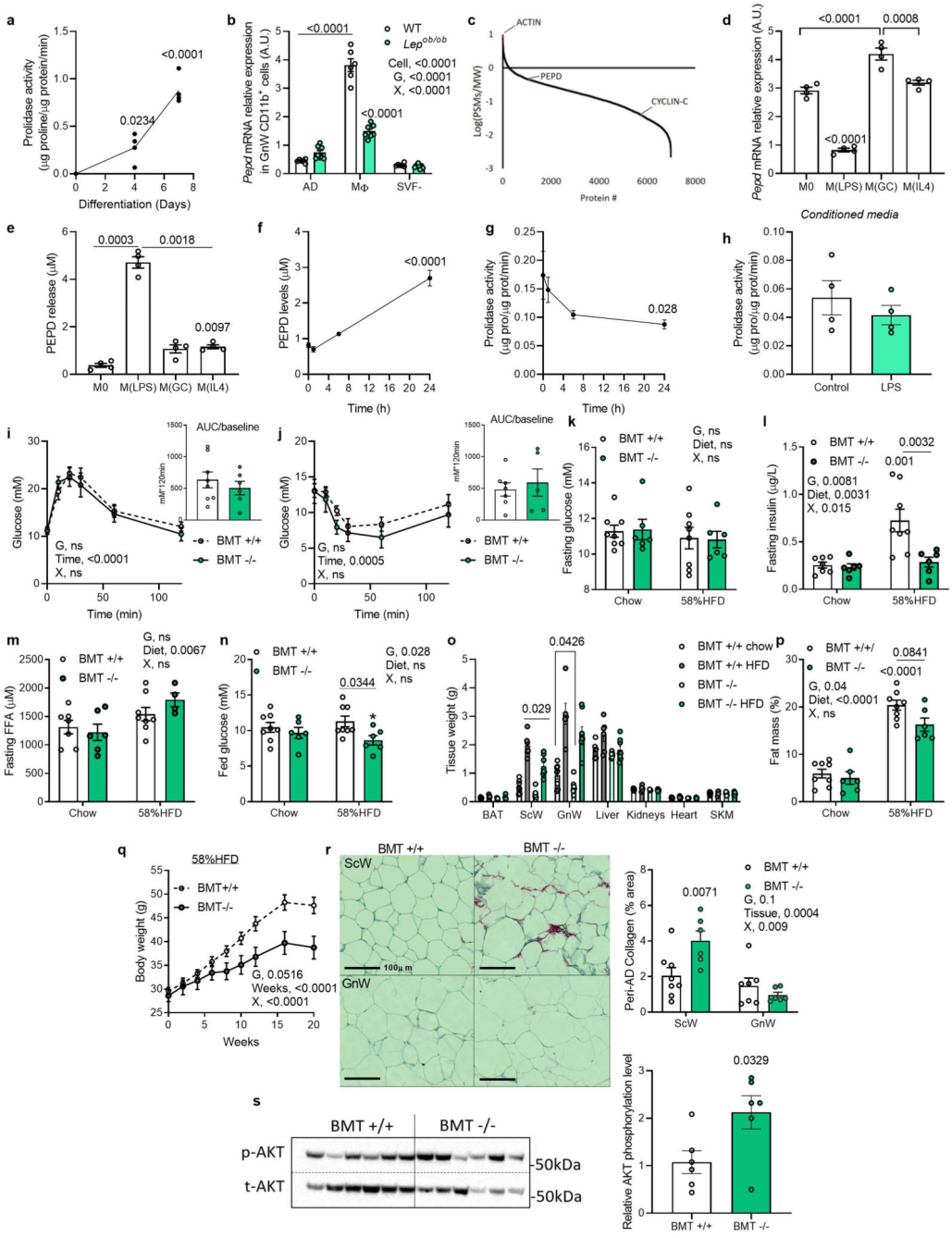

Extended Data Fig. 5. Pepd silencing in hematopoietic cells prevent obesity and associated metabolic disturbances.

a. Prolidase activity in BMDMs during differentiation (n=4 biologically independent samples). **b**. *Pepd* mRNA relative expression in adipocytes (AD), Mϕ (CD11b positive cells) and negative stroma-vascular fraction (SVF^{-}) isolated from GnW of WT (n=6) and $Lep^{Ob/Ob}$ mice (n=9). *compared to AD WT, # compared to Mϕ WT. **c**. Abundance of PEPD measured by mass spectrometry in unstimulated human iPS-derived Mϕ differentiated from FPS10C iPS line. Relative abundance of PEPD in comparison of other detected protein in

Europe PMC Funders Author Manuscripts

Europe PMC Funders Author Manuscripts

the same sample is plotted in the graph-where actin and cyclin are representing examples of high and low abundant proteins respectively. **d, e**. *Pepd* mRNA expression (d) or PEPD ELISA in culture media from BMDMs treated or not (M0) 6h (d) or 24 (e) with LPS, dexamethasone (GC) or IL4 (n=4 biologically independent samples). BMDMs were treated with LPS for 1,6 or 24h: **f, g**. PEPD level in culture media (f) and prolidase activity in BMDMs (g). **h**. Prolidase activity in culture media from BMDMs treated without (control) or with LPS (100ng/ml, 24h) (n=4 biologically independent samples). **I, j**. Blood glucose levels up to 120 min. after an intraperitoneal injection of glucose (2g/kg) in a glucose tolerance test (i) or insulin (0.75 IU/kg) in an insulin tolerance test (j) in BMT WT (n=8) and KO mice (n=6) fed chow. Respective AUC are represented. **k-n**. Fasting glucose (k), fasting insulin (l), fasting FFA (m) and fed glucose (n) blood levels in BMT-WT (n=8) mice compared to BMTKO mice (n=6) fed chow and HFD 58% (20 weeks). **. o, p**. Tissue weight (o) and Fat mass % (p) in BMT +/+ (n=8) and -/- (n=6) mice fed chow and HFD 58% for 20 weeks. **q**. Body weight curve in BMT-WT (n=8) mice compared to BMTKO mice (n=6) mice between 0 and 20 weeks HFD 58%. **r**. Representative images of red Sirius staining ScW and GnW from BMT-WT (n=8) mice compared to BMTKO mice (n=6) fed HFD 58% and quantification of peri-AD collagen represented as %. **s**. Representative images of blots and quantification of total and basal phosphorylated (Ser473) AKT in GnW of of BMT WT and KO mice fed HFD 58% (n=6/group). Data is presented as mean values +/- SEM. Data was analysed using a One way ANOVA followed by a Dunnett (a, f, g) or Tuckey (d, e) post-hoc multiple comparisons test, or using a 2-way ANOVA followed by a Tukey (b, k—p, r) or Sidak (I, j, q) post-hoc multiple comparisons test; G, genotype; X, interaction. A two-tailed Student's *t*-test was also used to analyse the data (h-j, s).

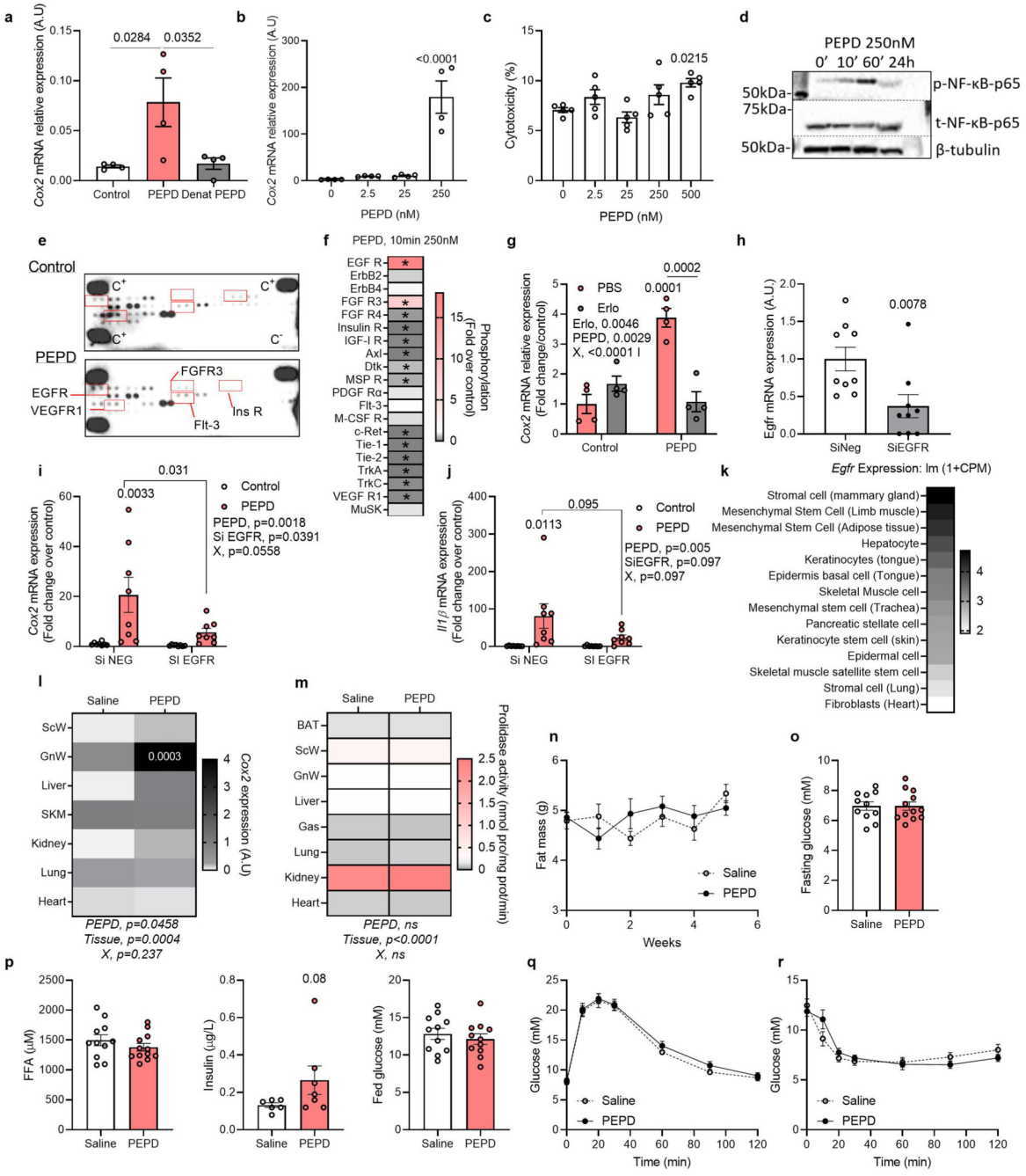

Extended Data Fig. 6. Purified PEPD protein promotes fibro-inflammation in macrophages through EGFR signalling

a. Cox2 mRNA relative expression in BMDMs treated or not (control) 4h with purified PEPD protein active or denaturated (denat PEPD) (n=3 biologically independent samples).**b**. Dose response effect of 4h treatment with purified PEPD protein on cox2 mRNA relative expression in BMDMs (n=4 biologically independent samples). **c**. % of cytotoxicity in BMDMs after 4h treatment with purified PEPD protein (n=4 biologically independent samples). **d**. Representative images of blots of total and phosphorylated (Ser 536) NF-

Europe PMC Funders Author Manuscripts

kB protein and beta-tubulin in BMDMs (n=4 biologically independent samples) treated with purified PEPD protein (0, 10, 60min or 24h, 250nM). **e, f**. Tyrosine-kinase receptor phospho-Array of multiple analytes (e) and quantification (f) of phosphorylation levels in cell extract from BMDMs treated without (control) or with purified PEPD protein (10 min, 250nM). Data from one experiment of a pool of 4 independent macrophage preparations. **g**. Cox2 mRNA relative expression in BMDMs (n=4 biologically independent samples) pre-treated (Erlo) or not (PBS) with Erlotinib 5μM, prior 24h treatment with (PEPD) or without (control) purified PEPD protein. * compared to control PBS, # compared to PEPD PBS. **h-j**. mRNA expression of Egfr (h), Cox2 (i) and Il1β (j) in RAW macrophages transfected with Si-EGFR or its negative control (Si-NEG) prior treatment with (PEPD) or without (control) purified PEPD protein (250nM,24h). **k**. Tissue and cell distribution of egfr expression from Tabula muris DataBase; **l, m**. Heat map of Cox2 mRNA expression (l) and prolidase activity (m) in different tissues from C57Bl/6 mice injected with saline or purified PEPD (n=11 biologically independent animals per group). **n-p**. Fat mass (n), fasting glucose (o), free fatty acids (FFA, p) and insulin levels (p), and fed glucose level (p) in PEPD-injected mice compared to controls (n=11 biologically independent animals per group). **q, r**. Blood glucose levels up to 120 minutes after an intraperitoneal injection of glucose (2g/kg) in a glucose tolerance test (q, IP-GTT) or insulin (0.75 IU/kg) in an insulin tolerance test (r, IP-ITT) in PEPD-injected mice compared to controls (n=11 biologically independent animals per group). Data is presented as mean values +/- SEM. Data was analysed using a One-way ANOVA followed by a Dunnett (b, c) or Tuckey (a) post-hoc multiple comparisons test, or using a 2-way ANOVA followed by a Tukey (g, I, j) or Sidak (l-n, q, r) post-hoc multiple comparisons test. A two-tailed Student's *t*-test was also used to analyse the data (h, o, p).

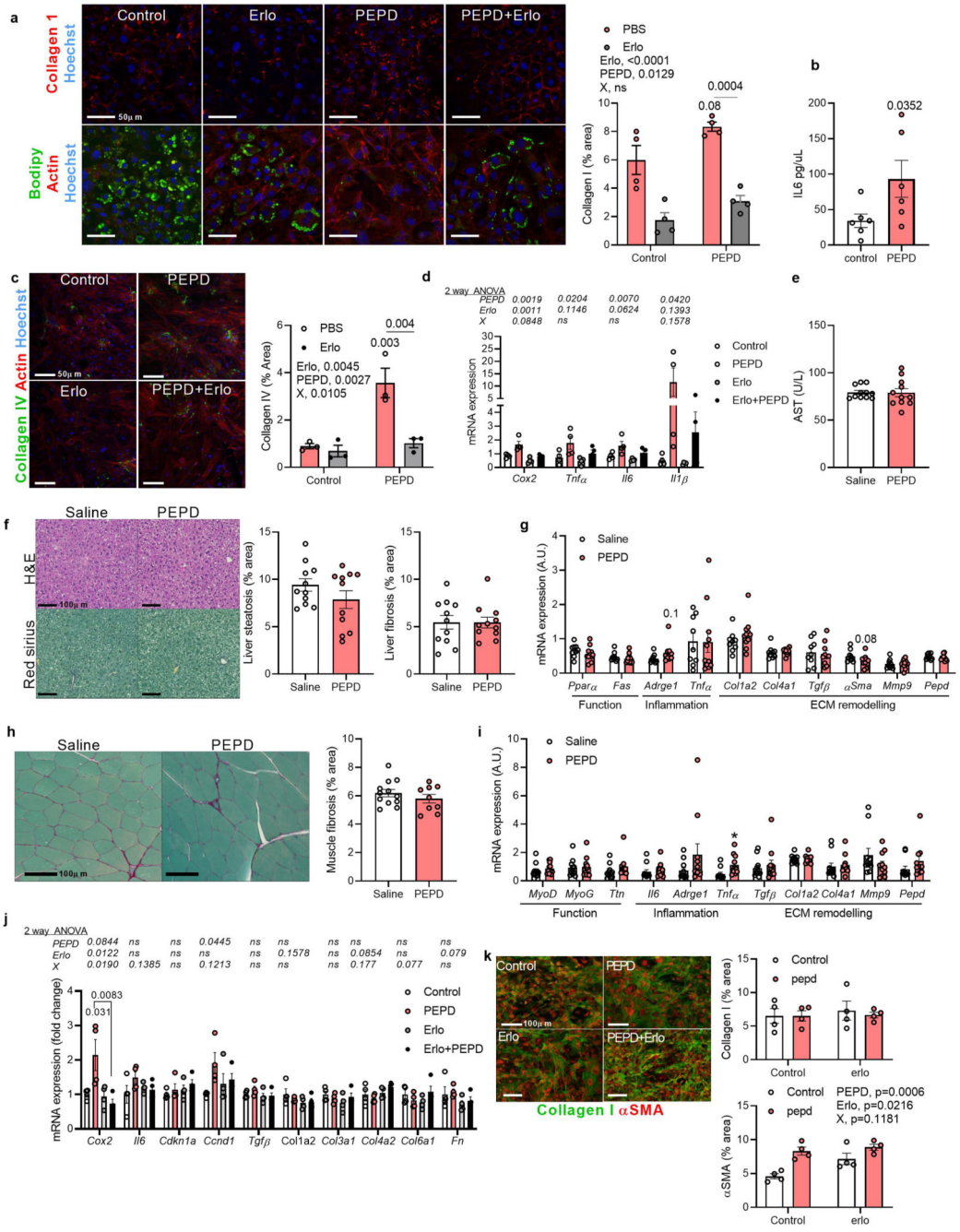

Extended Data Fig. 7. Purified PEPD protein promotes fibro-inflammation in pre-adipocytes and stellate cells through EGFR signaling.

a. Representative images of confocal analysis of anti-Collagen type I (in red,) and Bodipy staining (lipid accumulation in green) (i) and corresponding quantifications of collagen I staining (j) in 3T3-L1 adipocytes (n=4 biologically independent samples) pre-treated (Erlo) or not (PBS) with Erlotinib (5µM) prior treatment with (PEPD) or without (control) purified PEPD protein (250nM) during the first 5 days of adipogenic differentiation. * compared to control PBS, # compared to PEPD PBS. X, interaction. **b**. Il-6 level in culture media

Europe PMC Funders Author Manuscripts

of mature adipocytes isolated from ScW of C57Bl/6 mice treated or not (control) with purified PEPD protein (250nM, 24h, n=6 biologically independent animals per group). **c**. Representative images of confocal analysis of anti-Collagen type IV (in green,) and Actin staining (in red) and corresponding quantifications of collagen IV staining in stellate cells (n=3 biologically independent samples) pre-treated (Erlo) or not (PBS) with Erlotinib (5μM) prior treatment with (PEPD) or without (control) purified PEPD protein (250nM). **d**. Gene expression profile in stellate cells (n=4) pre-treated (Erlo) or not (PBS) with Erlotinib (5μM) prior treatment with (PEPD) or without (control) purified PEPD protein (250nM). **e**. AST serum level in PEPD-injected mice compared to controls (n=11/group). **f**. Representative images of H&E and Sirius staining in the liver from PEPD-injected mice compaired to control (n=11 biologically independent animals per group, a), and quantification of lipid droplet (steatosis) and collagen contents (fibrosis). g. Liver gene expression profile in PEPD-injected mice compared to controls (n=11 biologically independent animals per group). **h**. Representative images of red Sirius staining in gastrocnemius from PEPD-injected mice compaired to control (n=11 biologically independent animals per group), and quantification of collagen content (fibrosis). **i**. Gastrocnemius gene expression profile in PEPD-injected mice compared to controls (n=11 biologically independent animals per group). **j**. Gene expression profile in muscle fibroblasts pre-treated (Erlo) or not (PBS) with Erlotinib (5μM) prior treatment with (PEPD) or without (control) purified PEPD protein (250nM, 5 days). **k**. Representative images of confocal analysis of anti-Collagen type I (in green,) and αSMA staining (in red), and corresponding quantifications of collagen I and αSMA stainings in muscle fibroblasts (n=4 biologically independent samples) pre-treated (Erlo) or not (PBS) with Erlotinib (5μM) prior treatment with (PEPD) or without (control) purified PEPD protein (250nM, 5 days). Data is presented as mean values +/- SEM. Data was analysed using a 2-way ANOVA followed by aTukey post-hoc multiple comparisons test (a, c, d, j, k), or using a two-tailed Student's *t*-test (b, e-i).

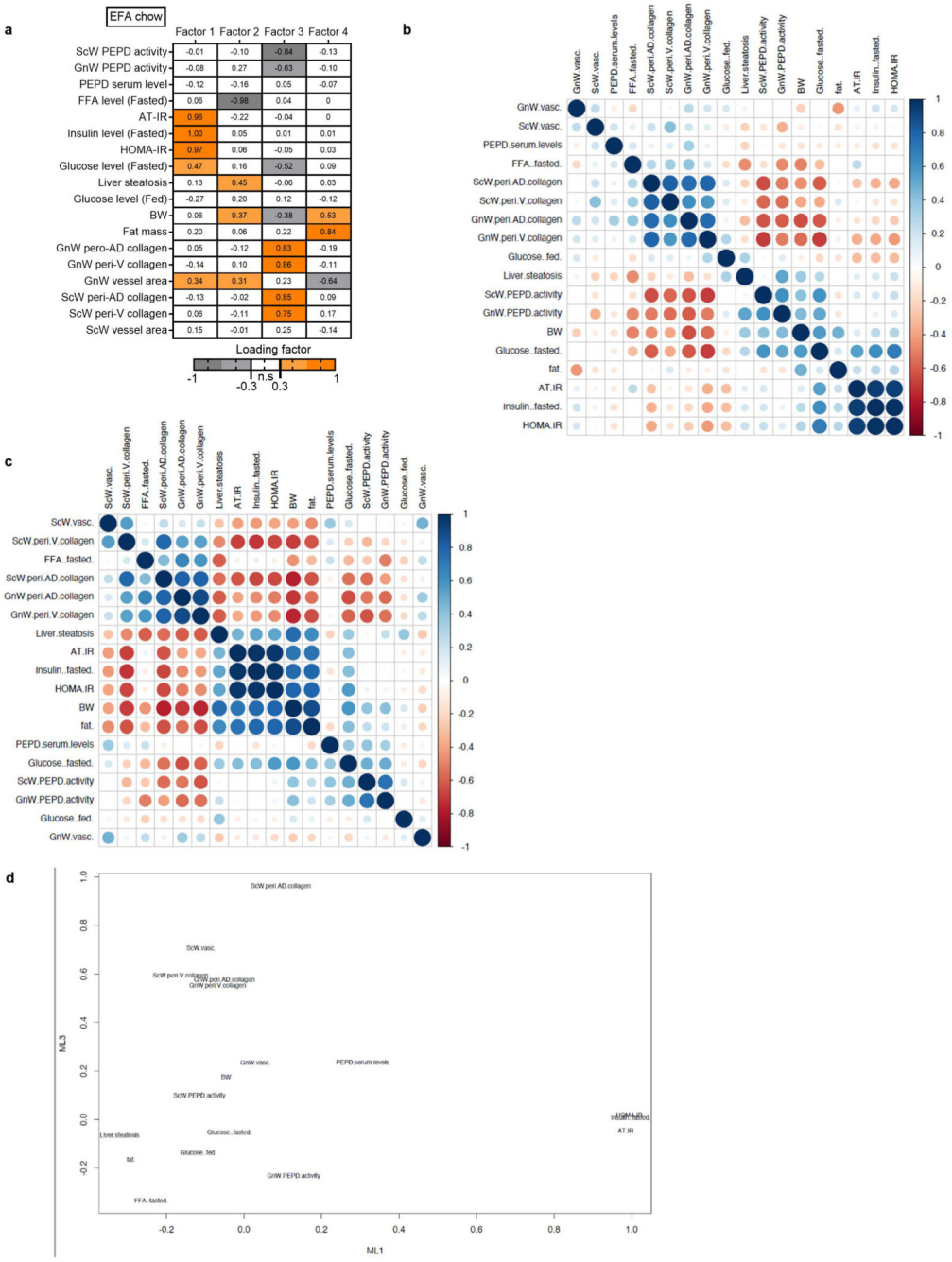

Extended Data Fig. 8. High PEPD serum levels is associated with AT insulin resistance and drives the differences between the pharmacologic and genetic animal models of PEPD down-regulation.

a. Heat map representing the four factors extracted through EFA performed among mice fed chow. The columns report the factors loadings of the observed variables. **b, c**. Pearson correlation matrix between ScW and GnW ECM remodelling markers, PEPD serum levels and metabolic parameters in the mice from the four models (PEPD, CBZ-Pro, BMT and PEPD-injection) fed chow (b) or chow+HFD (c). Metabolic/fibro-inflammatory parameters

Europe PMC Funders Author Manuscripts

from the four animal models (i.e. CBZ-Pro, PEPD, BMT and PEPD-injection) were plotted according to factor 1 and 3.

Supplementary Material

Refer to Web version on PubMed Central for supplementary material.

Acknowledgements

This work was funded by Wellcome-Trust strategic award [100574/Z/12/Z], MRC MDU (MC_UU_12012/2), H2020 EPoS (Elucidating Pathways of Steatohepatitis-Grant Agreement 634413) and the British Heart Foundation (RG/18/7/33636). The Disease Model Core, Biochemistry Assay Lab, the Histology Core and the Genomics and Transcriptomics Core are funded by MRC_MC_UU_12012/5 and a Wellcome-Trust Strategic Award [208363/Z/17/Z]. We thank the Wellcome-Trust Sanger Institute Mouse Genetics Project (Sanger MGP) and its funders for providing the mutant mouse line (Pepd<tm1a(KOMP)Wtsi). Funding and associated primary phenotypic information may be found at www.sanger.ac.UK/mouse portal. We thank the Disease Model Core from the Wellcome-MRC Institute of Metabolic Science and Agnes Lukasik for their technical assistance in animal work. All animal work was carried out in the Disease Model Core (MRC Metabolic Diseases Unit [MRC_MC_UU_12012/5]; Wellcome-Trust Strategic Award [100574/Z/12/Z]). We also thank Genomics and Transcriptomics core, the Histology core, and Gregory Strachan from the Imaging core for their technical assistance. All serum biochemistry was conducted by the Biochemistry Assay Lab (MRC Metabolic Diseases Unit [MRC_MC_UU_12012/5]). Clinical studies in France were supported by “Contrat de Recherche Clinic” (CRC APHP, Fibrota to JAW and KC), by the National Agency of Research (ANR-Captor to CR and KC) and by EFSD (to KC). H2020 EPoS funded KC (Elucidating Pathways of Steatohepatitis-Grant Agreement 634413). ARD, YHL, MD and MC were funded by MRC MDU (MRC_MC_UU_00014/5). MD also receives funding from the National Institute for Health Research [Cambridge Biomedical Research Centre at the Cambridge University Hospitals NHS Foundation Trust]. DC was supported by MRC MDU (MRC_MC_UU_12012/4). SC was supported by the ERC Senior Investigator award (669879). Wealso thank all the patients and their physicians, Dr. Laurent Genser for the surgical procedures, Prof Christine Poitou for patient recruitment and Dr Florence Marcheli for data management. Ruth JF Loos is supported by a grant from the NIH (R01DK107786). MdH is a fellow of the Swedish Heart-Lung Foundation (20170872) and a Kjell and Märta Beijer Foundation researcher. He is supported by project grants from the Swedish Heart-Lung Foundation (20140543, 20170678, 20180706) and the Swedish Research Council (2015-03657, 2019-01417).

We also want to acknowledge the FATBANK platform promoted by the CIBEROBN and the IDIBGI Biobank (Biobanc IDIBGI, B.0000872), integrated into the Spanish National Biobanks Network, for their collaboration and coordination.

The funders had no role in study design, data collection and interpretation, or submitting the work for publication.

Please note that the authors' views are those and not necessarily those of the NHS, the NIHR or the Department of Health and Social Care.

Data availability

All the raw data and uncropped immunoblots are available in Source Data files (Figures and immunoblots) and upon request (Extended Data Figures). DEGs and pathways from RNA-seq analysis can be found in Supplemental Tables. The RNA sequencing dataset is deposited in GEO under accession number GSE198358.

Code availability

Code is available On Github: https://github.com/bpucker/RNA-Seq_analysis. An Archive version is available in Zenodeo. The DOI (10.5281/zenodo.6192463) is displayed in the README on Github.

Europe PMC Funders Author Manuscripts

References

1. Sun K, Tordjman J, Clément K, Scherer PE. Fibrosis and adipose tissue dysfunction. Cell Metab. 2013; 18: 470–477. DOI: 10.1016/j.cmet.2013.06.016 [PubMed: 23954640]
2. Vidal-Puig A. Adipose tissue expandability, lipotoxicity and the metabolic syndrome. Endocrinol Nutr. 2013; 60 (Suppl 1) 39–43. [PubMed: 24490226]
3. Crewe C, An YA, Scherer PE. The ominous triad of adipose tissue dysfunction: inflammation, fibrosis, and impaired angiogenesis. J Clin Invest. 2017; 127: 74–82. DOI: 10.1172/JCI88883 [PubMed: 28045400]
4. Sorisky A, Molgat ASD, Gagnon A. Macrophage-induced adipose tissue dysfunction and the preadipocyte: should I stay (and differentiate) or should I go? Adv Nutr. 2013; 4: 67–75. DOI: 10.3945/an.112.003020 [PubMed: 23319125]
5. Abdennour M, et al. Association of Adipose Tissue and Liver Fibrosis with Tissue Stiffness in Morbid Obesity: Links with Diabetes and BMI Loss after Gastric Bypass. J Clin Endocrinol Metab. 2014. jc20133253 [PubMed: 24423338]
6. Pellegrinelli V, et al. Human adipocyte function is impacted by mechanical cues. J Pathol. 2014; 233: 183–195. [PubMed: 24623048]
7. Lavie CJ, De Schutter A, Milani RV. Healthy obese versus unhealthy lean: the obesity paradox. Nat Rev Endocrinol. 2015; 11: 55–62. [PubMed: 25265977]
8. Manning AK, et al. A genome-wide approach accounting for body mass index identifies genetic variants influencing fasting glycemic traits and insulin resistance. Nat Genet. 2012; 44: 659–669. DOI: 10.1038/ng.2274 [PubMed: 22581228]
9. Willer CJ, et al. Discovery and refinement of loci associated with lipid levels. Nat Genet. 2013; 45: 1274–1283. DOI: 10.1038/ng.2797 [PubMed: 24097068]
10. Kluth O, et al. Differential transcriptome analysis of diabetes-resistant and -sensitive mouse islets reveals significant overlap with human diabetes susceptibility genes. Diabetes. 2014; 63: 4230–4238. [PubMed: 25053586]
11. Yaghootkar H, et al. Genetic evidence for a normal-weight 'metabolically obese' phenotype linking insulin resistance, hypertension, coronary artery disease, and type 2 diabetes. Diabetes. 2014; 63: 4369–4377. DOI: 10.2337/db14-0318 [PubMed: 25048195]
12. Kitchener RL, Grunden AM. Prolidase function in proline metabolism and its medical and biotechnological applications. J Appl Microbiol. 2012; 113: 233–247. [PubMed: 22512465]
13. Rayment JH, Jobling R, Bowdin S, Cutz E, Dell SD. Prolidase deficiency diagnosed by whole exome sequencing in a child with pulmonary capillaritis. ERJ Open Res. 2019; 5 doi: 10.1183/23120541.00205-2018 [PubMed: 31041317]
14. Olivares O, et al. Collagen-derived proline promotes pancreatic ductal adenocarcinoma cell survival under nutrient limited conditions. Nat Commun. 2017; 8 16031 doi: 10.1038/ncomms16031 [PubMed: 28685754]
15. Yang L, et al. Prolidase directly binds and activates epidermal growth factor receptor and stimulates downstream signaling. J Biol Chem. 2013; 288: 2365–2375. DOI: 10.1074/jbc.M112.429159 [PubMed: 23212918]
16. Yang L, Li Y, Zhang Y. Identification of prolidase as a high affinity ligand of the ErbB2 receptor and its regulation of ErbB2 signaling and cell growth. Cell Death Dis. 2014; 5 e1211 doi: 10.1038/cddis.2014.187 [PubMed: 24810047]
17. Yang L, Li Y, Bhattacharya A, Zhang Y. A recombinant human protein targeting HER2 overcomes drug resistance in HER2-positive breast cancer. Sci Transl Med. 2019; 11 doi: 10.1126/scitranslmed.aav1620 [PubMed: 30674653]
18. Choi H, et al. Plasma Protein and MicroRNA Biomarkers of Insulin Resistance: A Network-Based Integrative -Omics Analysis. Front Physiol. 2019; 10: 379. doi: 10.3389/fphys.2019.00379 [PubMed: 31024340]
19. Lupi A, et al. N-benzyloxycarbonyl-L-proline: an in vitro and in vivo inhibitor of prolidase. Biochim Biophys Acta. 2005; 1744: 157–163. [PubMed: 15878628]

20. Small L, Brandon AE, Turner N, Cooney GJ. Modeling insulin resistance in rodents by alterations in diet: what have high-fat and high-calorie diets revealed? Am J Physiol Endocrinol Metab. 2018; 314: E251–E265. [PubMed: 29118016]
21. Søndergaard E, Espinosa De Ycaza AE, Morgan-Bathke M, Jensen MD. How to Measure Adipose Tissue Insulin Sensitivity. J Clin Endocrinol Metab. 2017; 102: 1193–1199. DOI: 10.1210/jc.2017-00047 [PubMed: 28323973]
22. Blohmke CJ, et al. Interferon-driven alterations of the host's amino acid metabolism in the pathogenesis of typhoid fever. J Exp Med. 2016; 213: 1061–1077. DOI: 10.1084/jem.20151025 [PubMed: 27217537]
23. Murray PJ, et al. Macrophage activation and polarization: nomenclature and experimental guidelines. Immunity. 2014; 41: 14–20. DOI: 10.1016/j.immuni.2014.06.008 [PubMed: 25035950]
24. Alasoo K, et al. Transcriptional profiling of macrophages derived from monocytes and iPS cells identifies a conserved response to LPS and novel alternative transcription. Sci Rep. 2015; 5 12524 doi: 10.1038/srep12524 [PubMed: 26224331]
25. Vila IK, et al. Immune cell Toll-like receptor 4 mediates the development of obesity- and endotoxemia-associated adipose tissue fibrosis. Cell Rep. 2014; 7: 1116–1129. [PubMed: 24794440]
26. Petkevicius K, et al. Accelerated phosphatidylcholine turnover in macrophages promotes adipose tissue inflammation in obesity. Elife. 2019; 8 e47990 doi: 10.7554/eLife.47990 [PubMed: 31418690]
27. Sharif O, et al. Beneficial Metabolic Effects of TREM2 in Obesity Are Uncoupled From Its Expression on Macrophages. Diabetes. 2021; 70: 2042–2057. DOI: 10.2337/db20-0572 [PubMed: 33627323]
28. Weisberg SP, et al. Obesity is associated with macrophage accumulation in adipose tissue. J Clin Invest. 2003; 112: 1796–1808. DOI: 10.1172/JCI19246 [PubMed: 14679176]
29. Tabula Muris Consortium. et al. Single-cell transcriptomics of 20 mouse organs creates a Tabula Muris. Nature. 2018; 562: 367–372. DOI: 10.1038/s41586-018-0590-4 [PubMed: 30283141]
30. Iwayama T, et al. PDGFRα signaling drives adipose tissue fibrosis by targeting progenitor cell plasticity. Genes Dev. 2015; 29: 1106–1119. DOI: 10.1101/gad.260554.115 [PubMed: 26019175]
31. Keophiphath M, et al. Macrophage-secreted factors promote a profibrotic phenotype in human preadipocytes. Mol Endocrinol. 2009; 23: 11–24. DOI: 10.1210/me.2008-0183 [PubMed: 18945811]
32. Liang B, et al. Characterization and proteomic analysis of ovarian cancer-derived exosomes. J Proteomics. 2013; 80: 171–182. [PubMed: 23333927]
33. Gonzales PA, et al. Large-scale proteomics and phosphoproteomics of urinary exosomes. J Am Soc Nephrol. 2009; 20: 363–379. DOI: 10.1681/ASN.2008040406 [PubMed: 19056867]
34. Kharaziha P, et al. Molecular profiling of prostate cancer derived exosomes may reveal a predictive signature for response to docetaxel. Oncotarget. 2015; 6: 21740–21754. DOI: 10.18632/oncotarget.3226 [PubMed: 25844599]
35. Lazar I, et al. Proteome characterization of melanoma exosomes reveals a specific signature for metastatic cell lines. Pigment Cell Melanoma Res. 2015; 28: 464–475. [PubMed: 25950383]
36. Yang L, Li Y, Bhattacharya A, Zhang Y. PEPD is a pivotal regulator of p53 tumor suppressor. Nat Commun. 2017; 8 2052 doi: 10.1038/s41467-017-02097-9 [PubMed: 29233996]
37. Surazynski A, Liu Y, Miltyk W, Phang JM. Nitric oxide regulates prolidase activity by serine/threonine phosphorylation. J Cell Biochem. 2005; 96: 1086–1094. [PubMed: 16167338]
38. Aslan M, Duzenli U, Esen R, Soyoral YU. Serum prolidase enzyme activity in obese subjects and its relationship with oxidative stress markers. Clin Chim Acta. 2017; 473: 186–190. [PubMed: 28867357]
39. Bel Lassen P, et al. The FAT Score, a Fibrosis Score of Adipose Tissue: Predicting Weight-Loss Outcome After Gastric Bypass. The Journal of Clinical Endocrinology & Metabolism. 2017; 102: 2443–2453. [PubMed: 28419237]
40. Yang L, Li Y, Bhattacharya A, Zhang Y. Inhibition of ERBB2-overexpressing Tumors by Recombinant Human Prolidase and Its Enzymatically Inactive Mutant. EBioMedicine. 2015; 2: 396–405. DOI: 10.1016/j.ebiom.2015.03.016 [PubMed: 26086037]

41. Roberts AW. G-CSF: a key regulator of neutrophil production, but that's not all! Growth Factors. 2005; 23: 33–41. [PubMed: 16019425]
42. Lacasa D, Taleb S, Keophiphath M, Miranville A, Clement K. Macrophage-secreted factors impair human adipogenesis: involvement of proinflammatory state in preadipocytes. Endocrinology. 2007; 148: 868–877. [PubMed: 17082259]
43. Besio R, et al. Improved prolidase activity assay allowed enzyme kinetic characterization and faster prolidase deficiency diagnosis. Clin Chim Acta. 2011; 412: 1814–1820. [PubMed: 21699887]
44. Myara I, Charpentier C, Lemonnier A. Optimal conditions for prolidase assay by proline colorimetric determination: application to iminodipeptiduria. Clin Chim Acta. 1982; 125: 193–205. [PubMed: 7139961]
45. Marcelin G, et al. A PDGFRα-Mediated Switch toward CD9(high) Adipocyte Progenitors Controls Obesity-Induced Adipose Tissue Fibrosis. Cell Metab. 2017; 25: 673–685. [PubMed: 28215843]
46. Moreno-Navarrete JM, et al. Insulin Resistance Modulates Iron-Related Proteins in Adipose Tissue. Dia Care. 2014; 37: 1092–1100. [PubMed: 24496804]
47. Reggio S, et al. Increased Basement Membrane Components in Adipose Tissue During Obesity: Links With TGFβ and Metabolic Phenotypes. The Journal of Clinical Endocrinology & Metabolism. 2016; 101: 2578–2587. [PubMed: 27049236]
48. Dobin A, et al. STAR: ultrafast universal RNA-seq aligner. Bioinformatics. 2013; 29: 15–21. DOI: 10.1093/bioinformatics/bts635 [PubMed: 23104886]
49. Haak M, et al. High Quality de Novo Transcriptome Assembly of Croton tiglium. Front Mol Biosci. 2018; 5: 62. doi: 10.3389/fmolb.2018.00062 [PubMed: 30027092]
50. Liao Y, Smyth GK, Shi W. The Subread aligner: fast, accurate and scalable read mapping by seed-and-vote. Nucleic Acids Res. 2013; 41 e108 doi: 10.1093/nar/gkt214 [PubMed: 23558742]
51. Love MI, Huber W, Anders S. Moderated estimation of fold change and dispersion for RNA-seq data with DESeq2. Genome Biol. 2014; 15: 550. doi: 10.1186/s13059-014-0550-8 [PubMed: 25516281]
52. Väremo L, Nielsen J, Nookaew I. Enriching the gene set analysis of genome-wide data by incorporating directionality of gene expression and combining statistical hypotheses and methods. Nucleic Acids Res. 2013; 41: 4378–4391. DOI: 10.1093/nar/gkt111 [PubMed: 23444143]
53. Liberzon A, et al. Molecular signatures database (MSigDB) 3.0. Bioinformatics. 2011; 27: 1739–1740. DOI: 10.1093/bioinformatics/btr260 [PubMed: 21546393]
54. Subramanian A, et al. Gene set enrichment analysis: a knowledge-based approach for interpreting genome-wide expression profiles. Proc Natl Acad Sci USA. 2005; 102: 15545–15550. DOI: 10.1073/pnas.0506580102 [PubMed: 16199517]
55. Grund B, Sabin C. Analysis of biomarker data: logs, odds ratios, and receiver operating characteristic curves. Curr Opin HIV AIDS. 2010; 5: 473–479. DOI: 10.1097/COH.0b013e32833ed742 [PubMed: 20978390]
56. Goksuluk, Dincer; Korkmaz, Selcuk; Zararsiz, Gokmen; Karaagaoglu, A Ergun. easyROC: An Interactive Web-tool for ROC Curve Analysis Using R Language Environment. The R Journal. 2016; 8/2
57. Yong AG, Pearce S. A Beginner's Guide to Factor Analysis: Focusing on Exploratory Factor Analysis. TQMP. 2013; 9: 79–94.
58. Revelle W. psych: Procedures for Psychological, Psychometric, and Personality Research. Northwestern University, Evanston, Illinois. R package version 219. 2021.
59. Lê S, Josse J, Husson F. FactoMineR : An R Package for Multivariate Analysis. J Stat Soft. 2008; 25
60. R Core Team. R Foundation for Statistical Computing. Vienna, Austria: 2020. https://www.R-project.org/

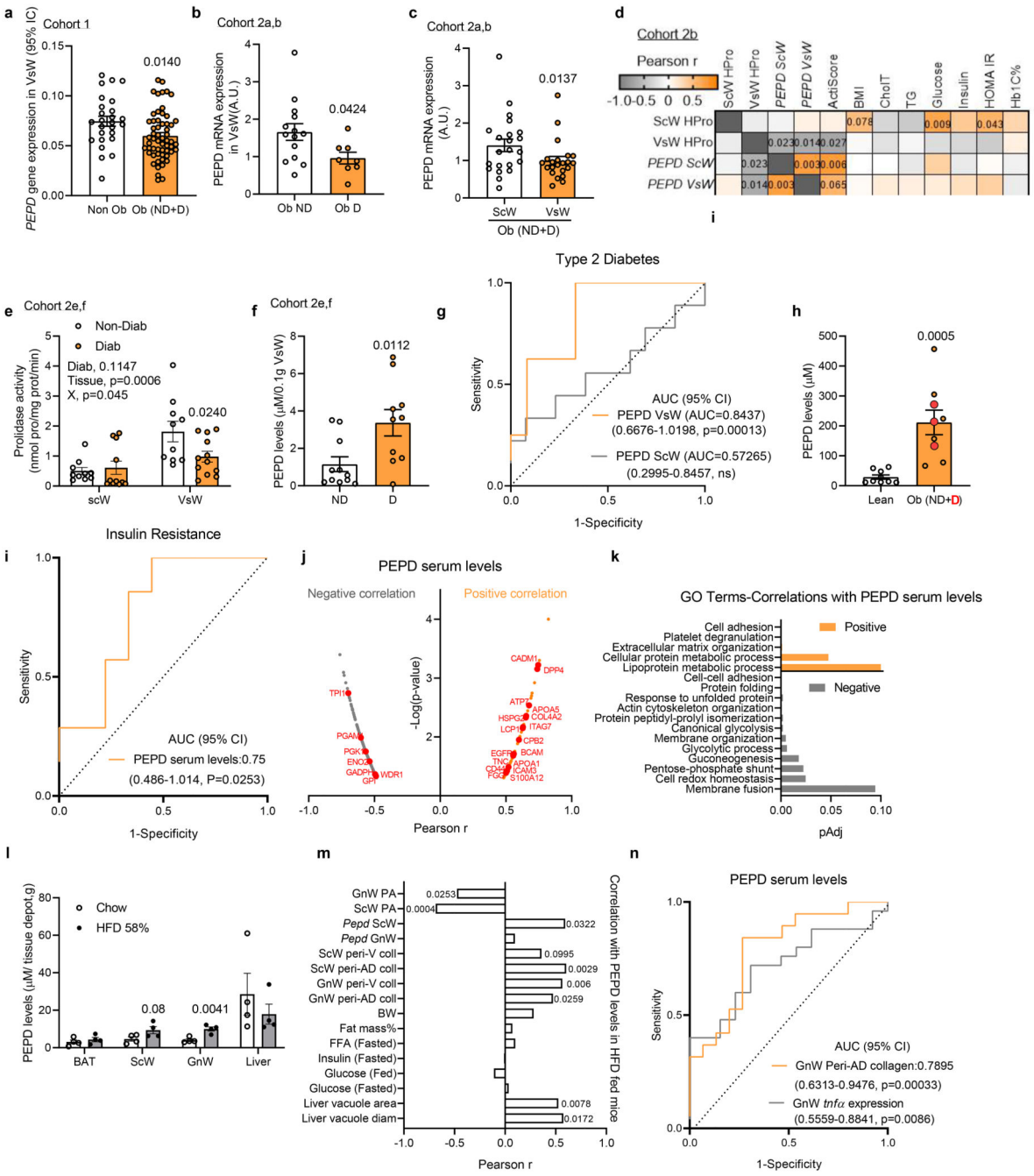

Figure 1. Obesity reduces AT PEPD activity and promotes PEPD release associated with AT fibrosis and insulin resistance.

a-c. *PEPD* gene expression in VsW from non-obese (n=26) and obese (n=58) subjects from cohort 1 (a), in ScW and VsW (visceral, omental depot) obese nondiabetic (Ob ND, 14) and diabetic (Ob D, n=8) subjects from cohort 2a, b (b, c). **d**. Pearson correlation matrix between ScW and VsW ECM remodelling markers and metabolic parameters in obese subjects from cohort 2b (n=14). **e**. Prolidase activity in ScW and VsW of obese diabetic (D, n=10) and non-diabetic(ND, n=12) subjects from cohort 2e, f. **f**. ELISA analysis of PEPD

Europe PMC Funders Author Manuscripts

levels from VsW explants medium of obese diabetic (D, n=9) and non-diabetic (ND, n=12) subjects from cohort 2e, f. **g**. Area under the receiver operating curve (AUC) values (95% CI) for PEPD VsW and ScW levels from cohort 2e, f to discriminate subjects with type 2 diabetes. **h**. ELISA analysis of PEPD levels in serum from lean (n=9) and obese nondiabetic (ND) or diabetic (D, red dots) (n=9) subjects from cohort 2d, e. **i**. Area under the receiver operating curve (AUC) values (95% CI) for PEPD serum levels from Hyungwon Choi *et al*. cohort[18]to discriminate subjects with insulin resistance. **j, k**. PEPD-protein correlations for Hyungwon Choi *et al*. cohort[18], shown as volcano plots (j) and GO enrichment analysis of the corresponding proteins (k). **l**. ELISA analysis of PEPD levels from tissue explants medium (i.e. BAT, ScW, GnW and liver) of C57/Bl6 mice fed chow or 20 weeks 58% HFD (n=4 biologically independent animals per group). **m**. Pearson correlations between PEPD serum levels and metabolic parameters in chow and HFD conditions (n=22 biologically independent animals). **n**. Area under the receiver operating curve (AUC) values (95% CI) for PEPD serum levels to predict a high degree of fibro-inflammation in GnW (i.e. GnW peri-AD collagen and GnW *Tnfα* expression) from mice fed chow and 58%HFD (n=34 biologically independent animals).

Data are presented as mean values +/- SEM.*p<0.05 compared to non-obese (a), Ob ND (b), ScW(c), ND (f), lean (h), chow (l) using a two-tailed Student's *t*-test. 2way ANOVA with Sidak's post-hoc multiple comparisons test has been performed; Diab, diabetic status; X, interaction (e).

Europe PMC Funders Author Manuscripts

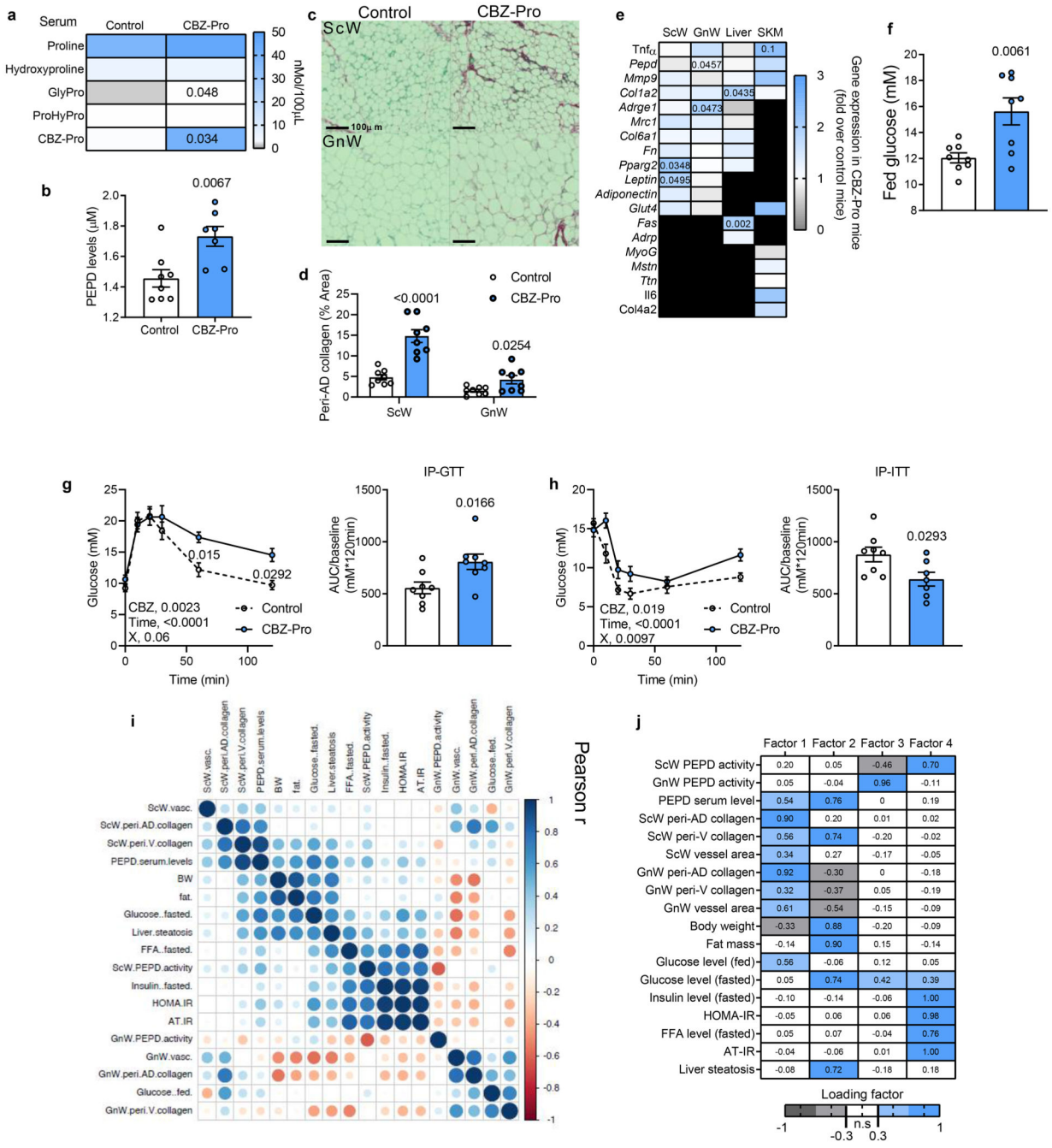

Figure 2. Pharmacological inhibition of PEPD promotes AT fibro-inflammation and insulin resistance in lean mice.

a, b, f. Proline metabolism-related amino acids serum level (a), PEPD serum levels (b) and fed glucose levels (f) in CBZ-Pro-treated mice and littermate's controls (n=8 biologically independent animals per group). **c, d**. Representative images of red Sirius staining in ScW and GnW of control and CBZ-Pro treated mice (n=8 biologically independent animals per group) (c) and corresponding quantification (d) of peri-adipocyte collagen deposition represented in % Area (peri-AD collagen). **g, h**. Blood glucose levels up to 120 minutes

Europe PMC Funders Author Manuscripts

after an intraperitoneal injection of glucose (2g/kg) in a glucose tolerance test (g) or insulin (0.75 IU/kg) in an insulin tolerance test (h) with the representative AUC (g) or AOC (h) in control and CBZ-Pro treated mice (n=8 biologically independent animals per group). i. Pearson correlations between ScW and GnW ECM remodelling markers, PEPD serum levels and metabolic parameters in control and CBZ-Pro-treated mice (n=16 biologically independent animals). **j**. Heat map representing the four factorsextracted through exploratory factor analysis. The columns report the factors loadings of the observed variables.
Data are presented as mean values +/- SEM. *p<0.05 compared to control (a, b, d-h) using a two-tailed Student's *t*-test. 2way ANOVA with Sidak's post-hoc multiple comparisons tests (g, h) has been used.

Europe PMC Funders Author Manuscripts

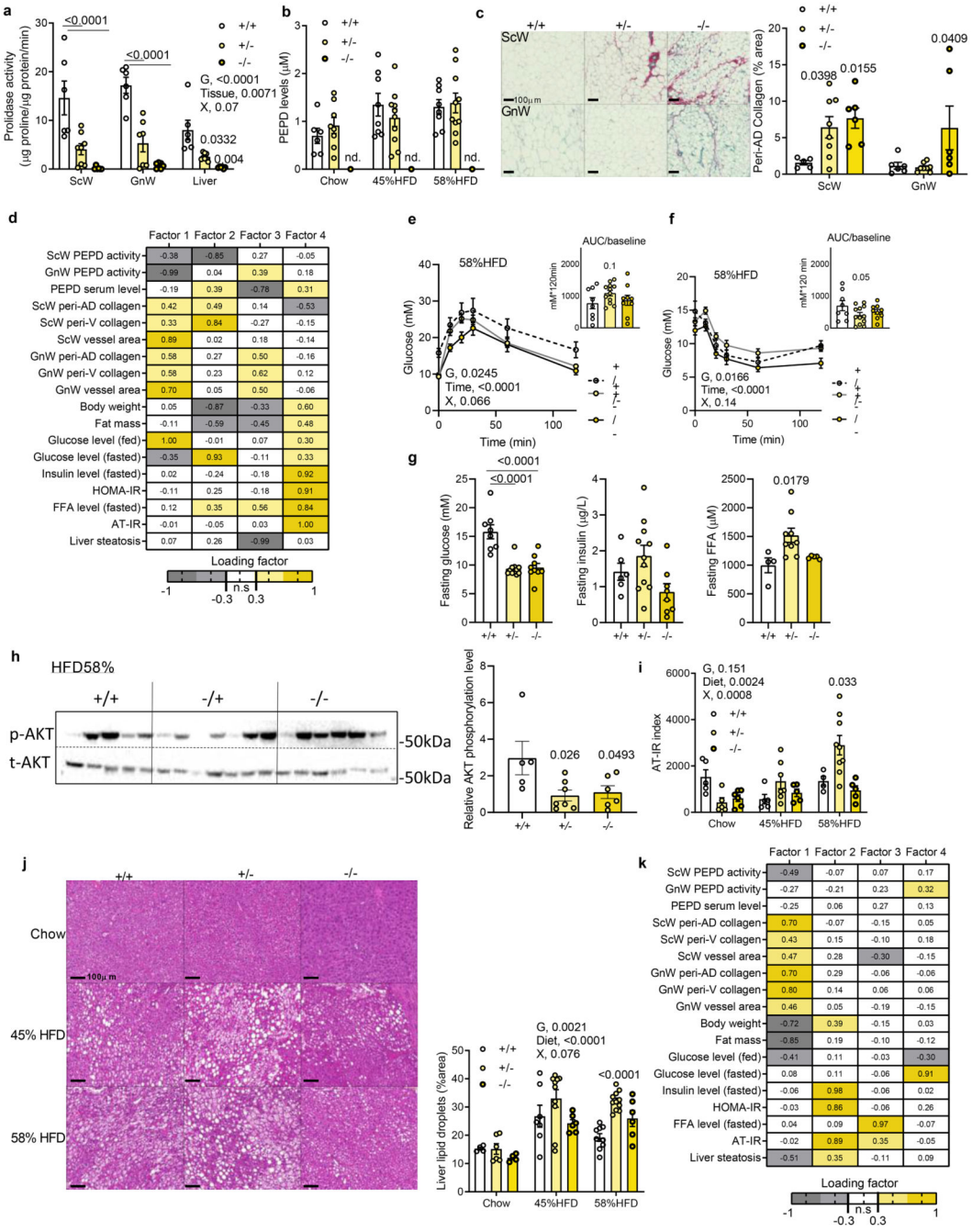

Figure 3. *Pepd* silencing exacerbates AT fibro-inflammation and metabolic dysfunctions in DIO mice.

a. Prolidase activity in ScW, GnW and liver from *pepd* WT (n=6), HET (n=8) and KO mice (n=5); **b**. ELISA analysis of PEPD levels in the serum of pepd WT (6) and HET (10) fed chow. **c**. Representative images of red Sirius staining in ScW and GnW from *pepd* WT (n=6), HET (n=8) and KO (n=6) mice fed chow and quantification of peri-adipocyte collagen % area (peri-AD collagen). **d, k**. Heat map representing the four factors extracted through exploratory factor analysis in *pepd* mice fed chow (d) and HFD58% (k). The

Europe PMC Funders Author Manuscripts

columns report the factors loadings of the observed variables. **e, f**. Blood glucose levels up to 120 min. after an intraperitoneal injection of glucose in a glucose tolerance test (e) or insulin (0.75 IU/kg) in an insulin tolerance test (f) with the representative AUC (e) or AOC (f) in *pepd* WT (n=8), HET (n=11) and KO (n=9) mice fed HFD 58%. **g**. Fasting glucose, insulin and FFA levels in *pepd* WT (n=8), HET (n=11) and KO (n=9) mice fed HFD 58%. **h**. Representative images of blots of total and phosphorylated (Ser 473) AKT protein and beta-Actin in GnW from *pepd* WT (n=8), HET (n-11) and KO (n=9) mice fed HFD 58%. **i**, AT-IR index in *pepd* WT, HET and KO mice in chow (n=6, 8, 6 biologically independent animals per group, respectively), 45%HFD (n=9, 11, 9 biologically independent animals per group, respectively) and HFD 58% conditions (n= 8,11,9 biologically independent animals per group, respectively). **j**, Representative images of H&E staining in liver from *pepd* WT, HET and KO mice fed chow (n=4, 6, 4, respectively), HFD 45% (n=7, 10, 6 biologically independent animals per group, respectively) and HFD 58% conditions (n= 9, 11, 6 biologically independent animals per group, respectively) and quantification of liver steatosis. **k**, Heat map representing the four factors extracted through exploratory factor analysis. The columns report the factors loadings of the observed variables.

Data are presented as mean values +/- SEM. Data have been analysed using 2way ANOVA with Turkey's post-hoc multiple comparisons test; G, genotype; X, interaction (a, b, e, f, i, j).*$p<0.05$ compared to +/+ using One way ANOVA with Sidak's (e, f) or Dunnett's (c, g, h) post-hoc multiple comparisons test.

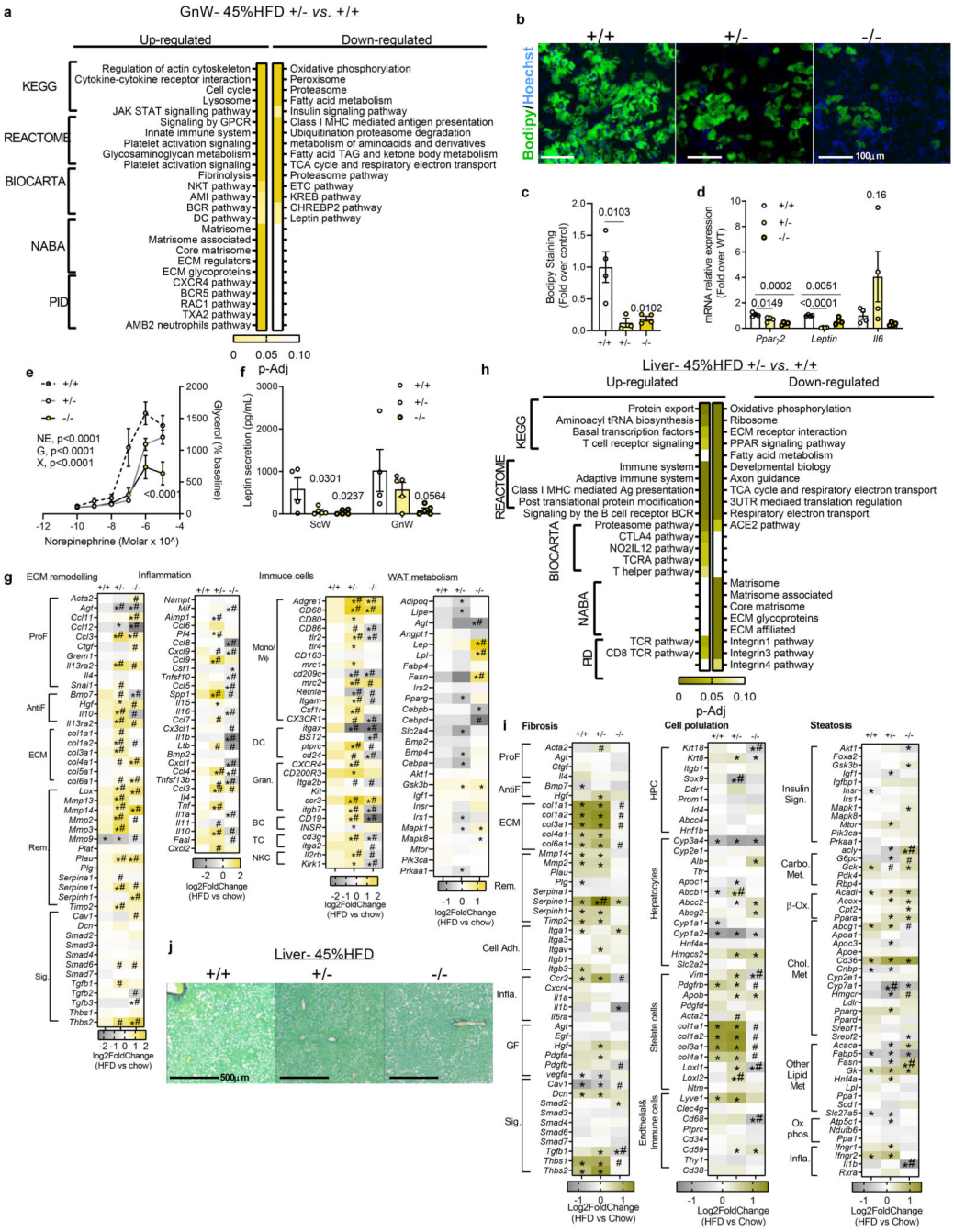

Figure 4. "Fibro-inflammatory" and "AT dysfunction"-related pathways are enriched in the GnW from *pepd* HET mice.

a, h. Pathway enrichment analysis of the DEGs in GnW (a) and liver (h) from *pepd* HET (C, n=10) and KO (D, n=9) mice compared to WT mice (n=8) fed HFD 45%, using different data bases (KEGG, Reactome, Biocarta, NABA and PID). The heat maps indicate the level of significant changes (false discovery rate-adjusted p-value). **b**, **c**. Representative image of confocal analysis (Bodipy staining in green, b) and quantification of lipid accumulation (c) in primary differentiated adipocytes isolated from GnW of *pepd* WT,

Europe PMC Funders Author Manuscripts

HET and KO mice (n=4 biologically independent animals per group). **d**. Gene expression in primary differentiated adipocytes isolated from GnW of *pepd* WT, HET and KO mice (n=4 biologically independent animals per group). **e**. Lipolytic dose-response curves for mature adipocytes isolated from GnW of from *pepd* WT (n=5), HET (n=7) and KO mice (n=6) in chow condition in response to 2h treatment with Norepinephrine. **f**. ELISA analysis of leptin secretion from ScW and GnW explants from *pepd* WT (n=4), HET (n=5) and KO (n=5) mice in chow condition. **g, i**. Heat maps of fibro-inflammatory- (g, i), metabolism- (g) and steatosis (i) -related DEGs in GnW (g) and liver (i) of *pepd* WT, HET and KO mice in HFD 45% (8, 10, 9 biologically independent animals per group, respectively) expressed as Log2 fold change (Log2FC) variation over chow diet (n=4, 8, 5 biologically independent animals per group, respectively). ProF (pro-fibrotic); AntiF (anti-fibrotic); Rem (ECM remodelling); Sig. (ECM-related signalling); Mono/Mϕ (monocyte/macrophage); DC (dendritic cell); Gran. (granulocyte); BC (B cell); TC (T cell); NKC (natural killer cell). **j**, Representative images of red Sirius staining in the liver from *pepd* WT (n=6), HET (n=8) and KO (n=6) mice fed HFD45%.

Data are presented as mean values +/- SEM. *p<0.05 compared to WT using One way ANOVA with Dunnett's post-hoc multiple comparisons test (c, d, f). 2way ANOVA with Turkey's post-hoc multiple comparisons test has been used (e). *p-Adj<0.1, significant DEG compared to chow diet. #q<0.05 compared to pepd WT (+/+). Statistical analysis of the RNAseq data is detailed in the methods section.

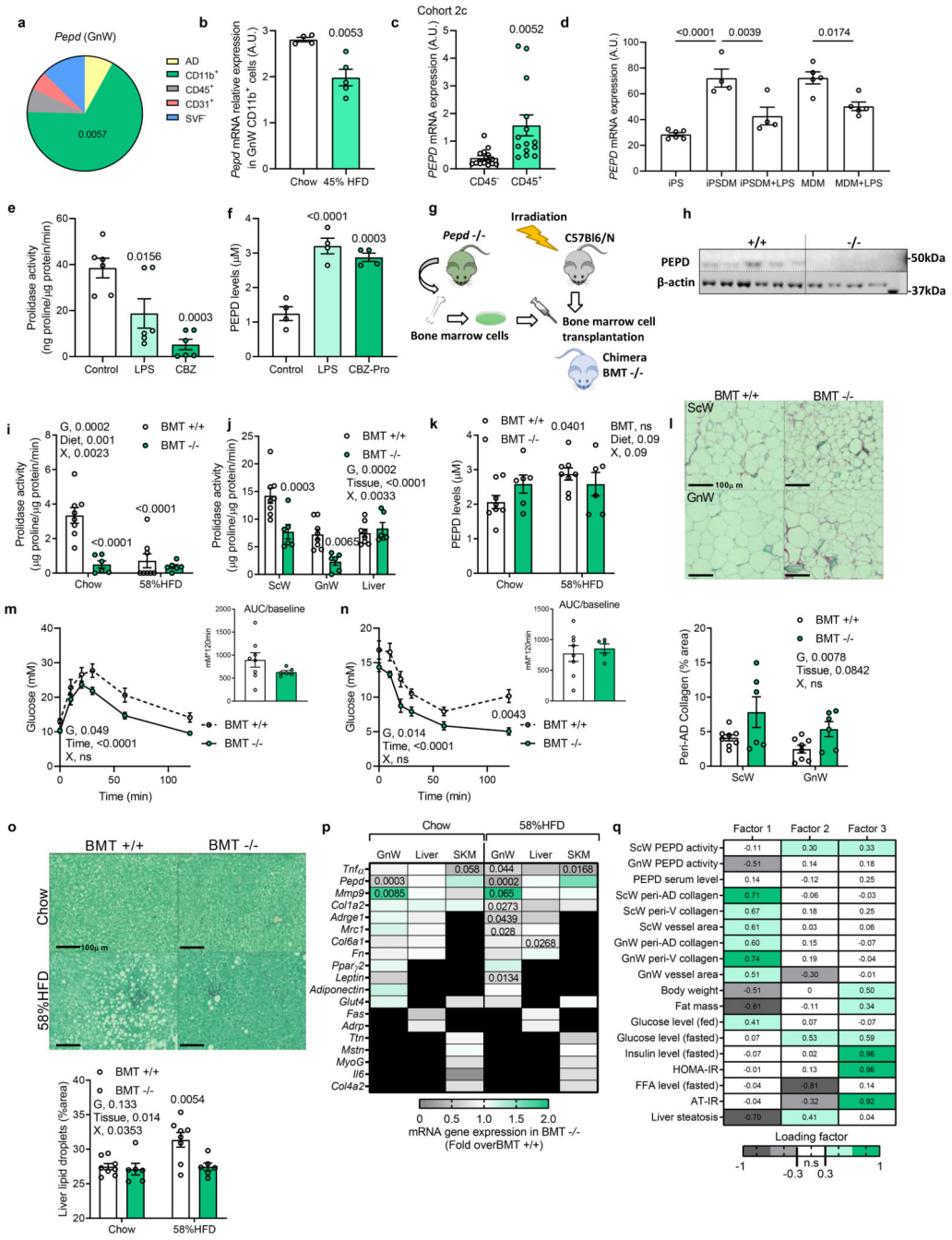

Figure 5. Hematopoietic-specific *pepd* silencing reduced AT fibro-inflammation and improved insulin sensitivity in obese mice.

a. Pie chart illustration of *Pepd* mRNA relative expression distribution in GnW from C57Bl/6 mice fed a chow diet (n=4 biologically independent animals). AD, adipocytes; $CD11b^+$, Mϕ; $CD45^+$, immune cells; $CD31^+$ endothelial cells and SVF^-, negative stroma-vascular fraction. **b**. *Pepd* mRNA relative expression in CD11b positive fraction (MΦ) of the GnW from C57Bl/6 mice fed chow (n=4) and HFD 45% (n=5) (20 weeks). **c**. *Pepd* mRNA relativeexpression in CD45+ and CD45- cells isolated from VsW of obese subjects

Europe PMC Funders Author Manuscripts

from cohort 2c (n=14 biologically independent samples). **d**. Global transcriptome of iPS cells (n=6), iPS-derived Mϕ (iPSDM, n=4), and monocyte-derived Mϕ MDM (n=5) were compared by RNAseq; and transcript per million (TPM) value of PEPD mRNA for each condition is plotted as bar diagram. iPSDM and MDM were treated with either 2.5 ng LPS for 6h or left untreated. **e, f**. Prolidase activity (e) and PEPD released level from BMDMs treated or not (control) 24h with LPS or CBZ-Pro (n=6 biologically independent samples per group).**g**. Scheme of the bone marrow transplant strategy. **h**, Representative image of western blot analysis of PEPD and Actin protein expression in BMDMs from pepd WT (n=5) and KO mice (n=4). i**, j**. Prolidase activity in peritoneal Mϕ (i), BAT, SCW, GnW, liver and SKM (gastrocnemius) (j) from BMT WT (n=8) mice compared to BMT KO mice (n=6). **k**. ELISA analysis of PEPD levels in the serum of BMT WT (n=8) and KO (n=6) mice fed chow and HFD 58%. **l**. Representative images of red Sirius staining ScW and GnW from BMT-WT (n=8) mice compared to BMTKO mice (n=6) fed chow and quantification of peri-AD collagen represented as %). **m, n**. Blood glucose levels up to 120 min. after an intraperitoneal injection of glucose (2g/kg) in a glucose tolerance test (m) or insulin (0.75 IU/kg) in an insulin tolerance test (n) in BMT WT (n=8) and KO mice (n=6) fed HFD 58% for 20 weeks. Respective AUC (m) or AOC (n) are represented**. o**. Representative images of red Sirius staining in Liver and quantification of liver steatosis expressed as % lipid droplets area in BMT WT (n=8) and KO mice (n=6) fed HFD 58% for 20 weeks. *Compared to BMT +/+ chow. #p<0.05 compared to BMT +/+ HFD 58%. **p**. Heat map of gene expression in GnW, liver and SKM (gastrocnemius) from BMTKO mice (n=6) fed chow and HFD 58% (20 weeks) expressed as fold change variation over BMT WT mice (n=8). q. Heat map representing the four factors extracted through exploratory factor analysis. The columns report the factors loadings of the observed variables.

Data are presented as mean values +/- SEM. *p<0.05, compared to AD (a), control (e, f) using a One way ANOVA with Dunnett's or Tukey's (d) post-hoc multiple comparisons test. *p<0.05 compared to chow (b, c), BMT +/+ (m, n, p) using a two-tailed Student's *t*-test. 2way ANOVA with Turkey's (I, o), Sidak's (j, l-n) or Dunnett's (k) multiple comparisons test have been used; G, genotype; X, interaction.

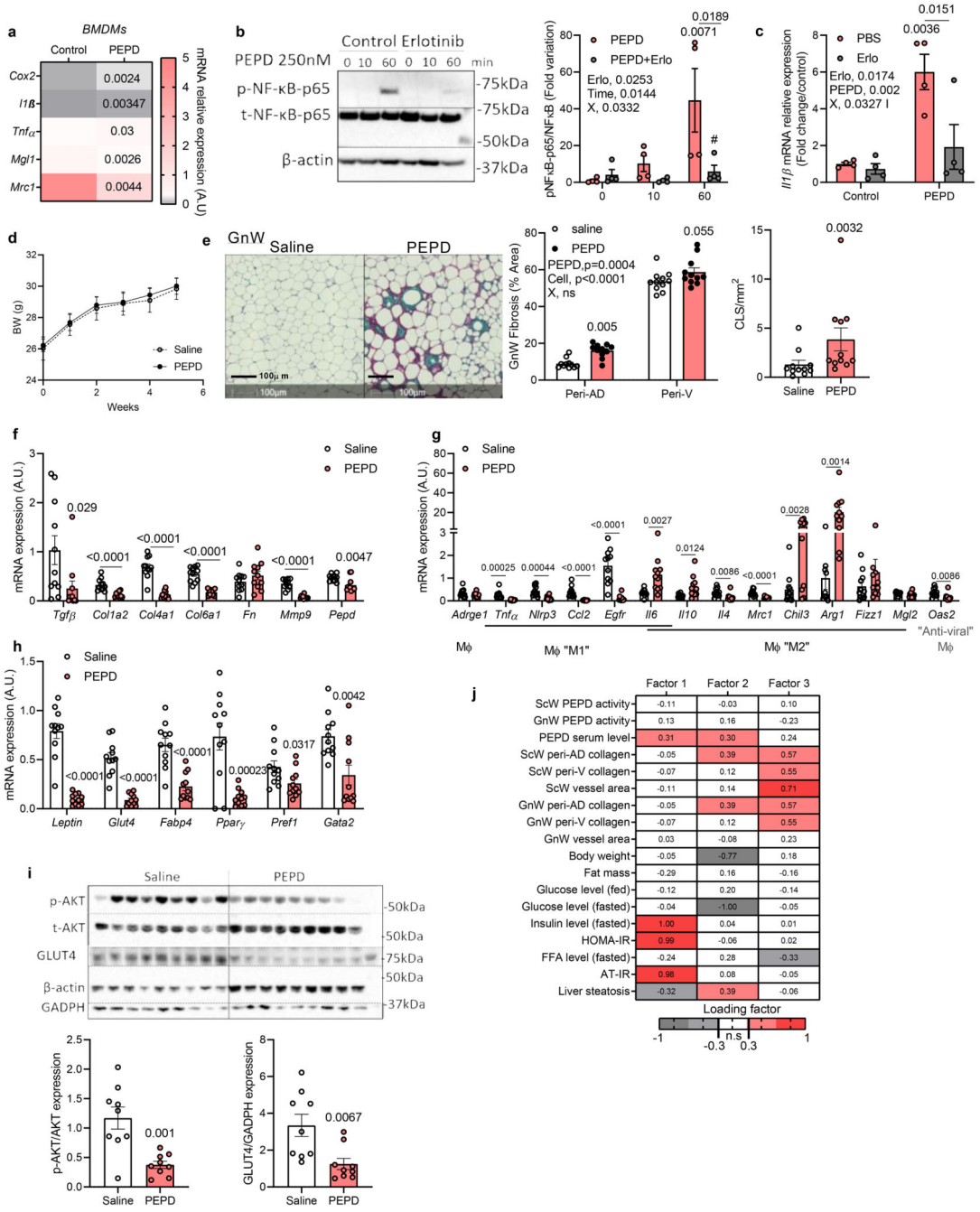

Figure 6. Purified PEPD protein induces fibro-inflammation and AT insulin resistance.

a. Heat map of gene expression in BMDMs after 4h treatment with purified PEPD protein (n=4 biologically independent samples). **b**. Representative images of blots and quantification of total andphosphorylated (Ser 536) NF-kB protein and beta-Actin in BMDMs (n=4 biologically independent samples) pre-treated or not with Erlotinib (Erlo, 5µM) prior treatment with purified PEPD protein (0, 10 and 60min, 250nM), and quantification. *compared to PEPD 0min, # compared to PEPD 60min. X, interaction. **c**. *IL1β* mRNA relative expression in BMDMs (n=4 biologically independent samples) pre-treated (Erlo)

Europe PMC Funders Author Manuscripts

or not (PBS) with Erlotinib 5μM prior treatment with (PEPD) or without (control) purified PEPD protein (250nM) for 24h. * compared to control PBS, # compared to PEPD PBS. **d**. Body weight curve in PEPD-treated mice compared to control (saline) mice (n=11 biologically independent animals per group) fed chow diet between 0 and 6 weeks treatment. **e**. Representative images of red Sirius staining in GnW PEPD-treated mice compared to control (saline) mice (n=11 biologically independent animals per group) fed chow diet and quantification of peri-AD collagen (represented as %) and crown like structures (CLS). **f-h**. mRNA expression of ECM remodelling (d), macrophage polarization markers (g) and adipocyte markers (h) in GnW (from PEPD-injected mice compared to controls (n=11 biologically independent animals per group). **i**. Representative images of blots of total and phosphorylated (Ser 473) AKT protein, GLUT4, GADPH and beta-Actin in GnW from PEPD-injected mice compared to controls (n=11 biologically independent animals per group). **j**. Heat map representing the four factors extracted through exploratory factor analysis. The columns report the factors loadings of the observed variables.
Data are presented as mean values +/- SEM. *$p<0.05$ compared to control (a) or saline (e-i) using a two-tailed Student's *t*-test. 2way ANOVA with Turkey's (b, c) or Sidak's (e) multiple comparisons test have been used; Erlo, Erlotinib; X, interaction.

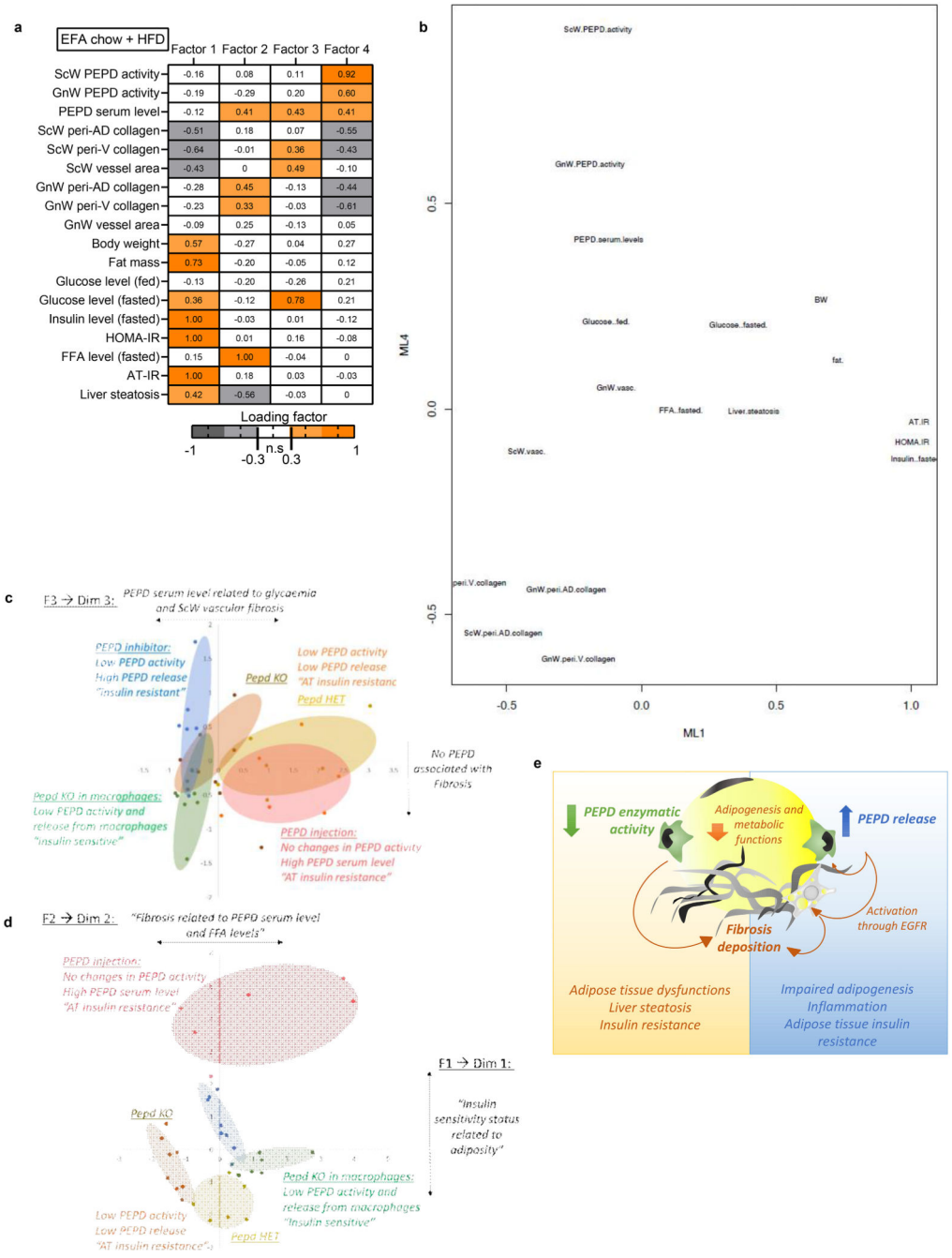

Figure 7. High PEPD serum levels are associated with AT insulin resistance and drives the differences between the pharmacologic and genetic animal models of PEPD down-regulation.

a. Heat map representing the four factors extracted through EFA performed among the mice from the four animal models (i.e. PEPD, CBZ-Pro, BMT and PEPD-injection) fed chow+HFD. The columns report the factors loadings of the observed variables. **b-d**. Metabolic/fibro-inflammatory parameters (b) and mice from the four animal models (i.e. CBZ-Pro, PEPD, BMT and PEPD-injection) (c) were plotted according to factor 1 and 4

Europe PMC Funders Author Manuscripts

(b), to factor 1 and 2 (c), or factor 3 and 4 (d). **e**. Summary of proposed roles of PEPD in obesity-associated AT dysfunctions and metabolic complications.

Europe PMC Funders Author Manuscripts

Europe PMC Funders Author Manuscripts

Table 1

Clinical parameters and bivariate correlations between *PEPD* gene expression and metabolic parameters in cohort 1 and 3

	Cohort 1				Cohort 3			
	VsW (n=84)		ScW (n=70)		VsW(n=46)		ScW (n=36)	
	r	*p*	*r*	*p*	*r*	*p*	*r*	*p*
Age (years)	**0.36**	***0.001***	0.05	*0.6*	0.21	*0.1*	-0.07	*0.6*
BMI (kg/m2)	**-0.34**	***0.002***	**0.25**	***0.04***	**-0.35**	***0.01***	0.13	0.4
Fasting glucose (mg/dl)	**0.31**	***0.005***	0.21	*0.08*	0.13	*0.4*	-0.14	*0.4*
Fasting triglycerides (mg/dl)	0.16	*0.1*	0.07	*0.5*				
***PLIN* (R.U.)**	**0.37**	***0.01***	**0.36**	***0.02***	**0.61**	***<0.0001***	0.22	*0.2*
***CIDEC* (R.U.)**	**0.32**	***0.03***	0.24	*0.1*	**0.63**	***<0.0001***	0.17	*0.3*
***ADRP* (R.U.)**	**0.37**	***0.01***	0.08	*0.6*	0.13	*0.4*	-0.23	*0.1*
***TIP47* (R.U.)**	**0.4**	***0.006***	0.21	*0.1*	**0.69**	***<0.0001***	0.22	*0.1*
***PPARG* (R.U.)**	**0.51**	**<0.0001**	0.09	*0.5*	0.28	*0.07*	0.07	*0.7*
***FASN* (R.U.)**	0.16	*0.1*	-0.09	*0.5*	0.05	*0.7*	0.24	*0.1*
***TNFα* (R.U.)**	0.1	*0.4*	-0.04	*0.7*	0.21	*0.2*	0.27	*0.1*
***COL6A3* (R.U.)**	0.1	*0.4*	0.03	*0.8*				
***COL6A6* (R.U.)**	-0.19	*0.1*	0.1	*0.6*				
***CD68* (R.U.)**	**0.23**	***0.05***	0.1	*0.4*				
***EGFR* (R.U.)**	**0.22**	***0.05***	-0.18	*0.2*	**0.37**	***0.02***	-0.02	*0.9*
***COL4A1* (R.U.)**					**0.36**	***0.02***	0.02	*0.9*
***GLUT4* (R.U.)**					**0.55**	***<0.0001***	0.16	*0.3*
(R.U.)					-0.08	*0.6*	-0.07	*0.7*
***ADIPOQ* (R.U.)**					**0.33**	***0.03***	-0.02	*0.8*